Advances in Civil Engineering Materials

doi:10.1520/ACEM20230031 / Vol. 13 / No. 1 / 2024 / available online at www.astm.org

Ekkeri Prakash Sumukh,[1] Bibhuti Bhusan Das,[2] and Salim Barbhuiya[3]

Effect of Iron Ore and Copper Ore Tailings on Engineering Properties and Hydration Products of Sustainable Cement Mortar

Reference

E. P. Sumukh, B. B. Das, and S. Barbhuiya, "Effect of Iron Ore and Copper Ore Tailings on Engineering Properties and Hydration Products of Sustainable Cement Mortar," *Advances in Civil Engineering Materials* 13, no. 1 (2024): 50–75. https://doi.org/10.1520/ACEM20230031

ABSTRACT

The prohibition of river sand mining has drawn the attention of researchers in finding practicable alternatives. In the approach of finding these alternatives, it is essential to ensure minimal or zero impairment to the ecological balance, which can be mainly attained by making use of industrial waste/byproducts. The wastes from the mining industry are the major contributors in causing impairment to the environment, and their influence on the stability of mortars on using as fine aggregates needs to be systematically investigated with the view of long-term performance concerns. Thus, the present study explores the applicability of mine tailings and finding the optimum dosage in cement mortars by investigating the engineering properties and microstructure development with the aid of qualitative and quantitative analysis associated with hydration products. The studies confirm that the increased consumption of portlandite for secondary hydration reactions followed by the additional formation of calcium silicate hydrate (CSH) and calcium aluminum silicate hydrate (CASH) phases in mine tailing-based mortars helped in achieving a quality microstructure. These additional formations of CSH and CASH phases are also confirmed through Fourier transform infrared spectroscopy by identifying the shift of Si-O-Si stretching vibration bands toward a lower wavenumber. The lowering of calcium/silicate atomic ratio and increased formation of mineralogical compounds related to CSH and CASH in x-ray diffraction patterns also confirms the same. Gismondine, chabazite, and hillebrandite are the additional phases formed and found to take part in refining the pore structure. This enhanced performance of mine tailing mortars was also verified with the aid of a modified Andreasen and Andersen particle packing model. The formation of high-quality microstructure is reflected in the hardened properties of optimized cement mortar in the proportion of 20 % for iron ore tailing and 30 % for copper ore tailing.

Manuscript received April 17, 2023; accepted for publication January 16, 2024; published online March 25, 2024. Issue published March 25, 2024.

[1] Sustainable Construction and Building Materials Laboratory, Department of Civil Engineering, National Institute of Technology Karnataka, Surathkal, Karnataka 575 025, India, https://orcid.org/0000-0002-1393-6639

[2] Department of Civil Engineering, National Institute of Technology Karnataka, Surathkal, Mangaluru 575 025, India (Corresponding author), e-mail: bibhutibhusan@gmail.com, https://orcid.org/0000-0002-1245-4494

[3] Department of Engineering and Construction, University of East London, London E16 2RD, UK, https://orcid.org/0000-0002-4325-281X

Keywords

mine tailings, mortar, hydration, particle packing, microstructure, characterization, sustainability

Introduction

With the ever-increasing quantities of industrial byproducts and waste materials produced worldwide, solid waste management has become a major environmental concern. Discharging industrial wastes such as mine tailings into the environment has a greater ability to cause environmental hazards that can pose a substantial health risk to all creatures. In India, the mining industry is one of the most important contributors to the national economy. The principal minerals found in the country include bauxite, chromite, copper, diamonds, dolomite, fluorite, graphite, gold, iron ore, limestone, etc. Waste materials are generated in abundant quantity during the mining of minerals and ores. Because they are no longer useful to mine owners, after the extraction of required material, tailings are dumped in the surroundings, which occupy a large amount of land. If not properly maintained, they cause some major hazards to the environment in the form of land degradation, fire hazards, water pollution, and air pollution because of the presence of toxic and combustible compositions.[1–5] But maintaining the stability of these dumps is also a major challenge for the mining industry. It has been reported that the quantity of tailings generation went up to 90–98 % for copper ore and 20–50 % for other minerals.[6–8] Thus, huge quantities of tailings are being generated from different sources such as copper ore, bauxite ore, iron ore, and gold ore, which are estimated to be 4.06 billion kgs, 2.74 trillion kgs, 294.65 billion kgs and around 1,000 kgs, respectively, per annum.[9,10]

Because of the lack of landfill space and its high cost, the usage of these mine tailings in some applications has become increasingly essential. However, the effective approach for the application of these mine tailings is not being suitably developed.[1,2,5] Thus, there is a potential need to utilize these mine tailings in an effective manner in different fields like construction, pavements, backfilling, etc. Whereas on the other hand, river sand mining has been prohibited in many provinces because of the adverse impacts causing ecological imbalances in the environment. But natural river sand has been widely accepted as a conventional fine aggregate in the production of cement mortars. As of now, fine crushed granite rocks (manufactured sand, i.e., M-Sand) have largely replaced river sand in the construction industry. Even though M-Sand showed satisfying performance as an alternative to river sand, it has certain disadvantages in fulfilling the performance requirements of concrete such as grading requirements, workability,[11] surface finishing ability,[12] compressive strength, density, yield, etc. Moreover, the problems associated with river sand extraction are far more destructive than mining of granite rocks, which is being widely accepted as coarse aggregate in producing concrete.[13,14] Thus, the production of concrete and mortars using mine tailings is the best possible option when these tailings can be employed sustainably as an alternative ingredient to river sand. The use of these mine tailings as a replacement for conventional materials can not only provide an abundant and cheap source of raw materials for concrete or mortar but also minimize pollutants and improve sustainability credentials.

The application of mine tailings as a replacement for river sand in the cementitious system has been investigated by the researchers, who witnessed a satisfactory performance as the mine tailings were usually in a well-graded state with particle size distribution (PSD) being quite similar to river sand. Previous studies have also revealed that the utilization of mine tailings is economical, efficient, and socially beneficial and improves the environmental situation.[15–18] The hardened properties of iron ore tailing (IOT)–based cementitious composites were reported to increase till 25 %,[19] 25–40 %,[20] 35 %,[21] 50 %,[18] and even 100 %[22] replacement of river sand. Studies have also reported that density of cementitious composites increases with the usage of mine tailings in the presence of heavy metals.[15,18,20,23,24] However, the workability and durability characteristics were reported to reduce with the usage of IOT.[18–20,22]

The workability characteristics of cementitious composites were found to be enhanced by the usage of copper ore tailing (COT) because of its particle morphology.[15] Previous studies have also witnessed a slight improvement in the hardened properties of COT-based cementitious composites till 10–20 %,[23,24] 60 %,[25] and even 100 %[26] replacement of river sand. In contrast to this, there is a study claiming the hardened properties are reduced with

the usage of COT.[15] In addition to these, some studies have also confirmed the durability characteristics are reduced by the usage of COT.[23,24] These observed hindrances were primarily attributed to inferior physical properties and grading requirements of mine tailings in comparison with the conventional river sand.[15]

However, a great deal of variability was observed in the reported values of engineering properties in the case of cementitious composites produced by using mine tailings. Each of them showed a different impact on the mechanical properties and long-term durability of the resulting cement mortar. The influence of using mine tailings followed by the mechanism that alters the engineering properties of cement mortar were not thoroughly investigated in the available literature. In addition, the characterization studies on these mine tailing–based cement mortars were found to be very limited in the literature, and it is the need of the hour to understand because it is very much essential in assessing the long-term behavior and bridging future research. Hence, the present study aims to comprehensively investigate the influence of using mine tailings as a substitute material to river sand through experimental investigations and characterization techniques. Thus, an attempt has been made to discuss the physical and chemical mechanism that occurs in the cementitious system upon the usage of mine tailings that prerequisite the clear understanding of material, engineering, microstructure, and durability properties of cement mortar. Consequently, the present study contributes to developing a sustainable solution for the problems associated with the waste management of COT and IOT by effectively using them as an alternative to conventional fine aggregates in practice as a way toward achieving sustainability.

Materials and Experimental Methodology

MATERIALS USED AND THEIR PROPERTIES

The binder used for the production of cement mortar was 53 grade ordinary portland cement (OPC 53G) conforming to ASTM C150/C150M-22, *Standard Specification for Portland Cement*.[27] Locally available normal potable water conforming to IS 10500:2012, *Drinking Water Specifications*,[28] was used for mixing and curing of mortar specimens. Natural river sand falling under zone II of IS 383-2016, *Specification for Coarse and Fine Aggregate from Natural Sources for Concrete*,[29] was utilized as fine aggregate, and polycarboxylate ether–based superplasticizer conforming to IS 2645:2003, *Specification for Integral Waterproofing Compounds for Cement Mortar and Concrete-Specification*,[30] and IS 9103:1999, *Specification for Concrete Admixtures*,[31] was employed to achieve the required flow characteristics in the produced cement mortar. The study mainly highlights the effective utilization of two varieties of mine tailings such as IOT and copper ore tailings (COT) as possible alternatives to river sand.

Various tests were conducted as per the standards to extract the properties of materials used, and the observed results are tabulated in **Table 1**. **Figure 1A** presents their PSD. The PSD data show that a significant volume of finer fractions (less than 150 μm) were present in mine tailings (11.6 % in IOT and 9.9 % in COT). The finer

TABLE 1
Properties of various materials used in the study

		Materials				
Properties		OPC	RS	IOT	COT	SP
Specific gravity		3.11	2.59	3.32	2.39	1.08 ± 0.02
Fineness, m^2/kg		300	…	…	…	…
Bulk density, kg/m^3	Loose	…	1,500	1,733	1,372	…
	Compacted	…	1,598	1,925	1,575	…
% of voids	Loose		43.07	47.71	42.61	…
	Compacted	…	39.34	41.93	34.10	…
Fineness modulus		…	2.47	2.32	1.74	…
Water absorption, %		…	0.98	0.66	0.79	…

Note: RS = river sand; SP = superplasticizer.

FIG. 1 (*A*) PSD of various materials used; (*B*) mineralogical composition of fine aggregates used.

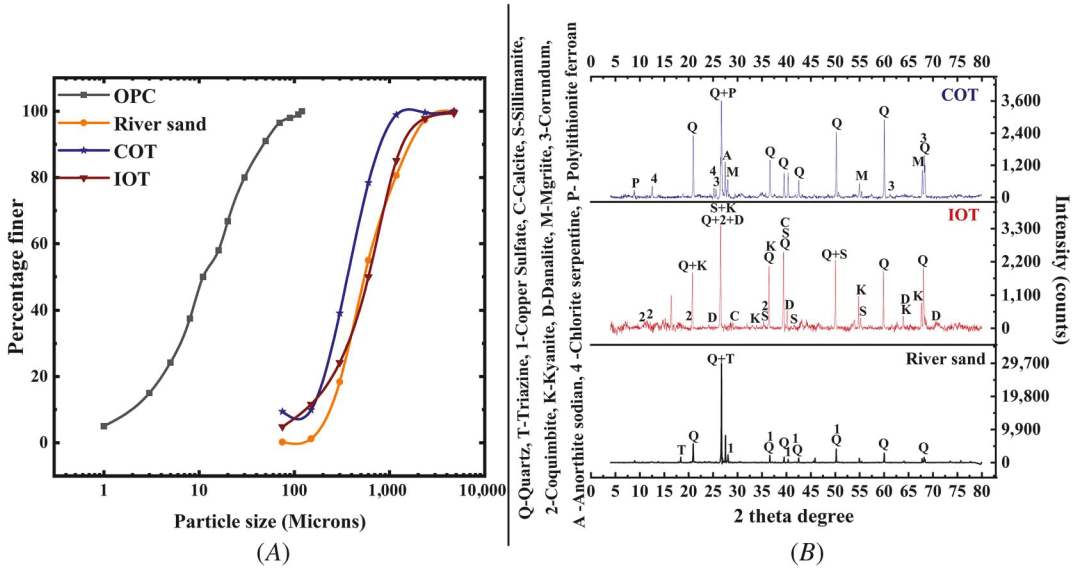

fractions of size below 75 μm were found to be 9.4 % in COT and 4.8 % in IOT. Figure 1*B* presents the x-ray diffraction (XRD) patterns of fine aggregates used, which highlights their mineralogical compositions and particle geometry. The XRD patterns of river sand show highly crystalline geometry predominantly with quartz and traces of copper sulfate and triazene in it. However, the tailing particles showed a comparatively more amorphous structure than river sand because of the presence of reactive minerals in them. The lower intensity range of XRD peaks in tailing particles compared with that of river sand confirms the lower crystallinity of mine tailings. The analysis shows that the IOT has aluminosilicate minerals (Al_2SiO_5), such as sillimanite and kyanite. Iron-based minerals, such as coquimbite and danalite, were also detected through XRD analysis. Similarly, the COT shows aluminosilicate minerals such as polylithionite, anthorite ($CaAl_2Si_2O_8$), chlorite, and traces of copper-based mineral mgriite. A similar kind of structural geometry was obtained in the past studies conducted on IOT[19,22] and COT particles.[32–34]

The morphology of the tailing particles was studied by conducting scanning electron microscopy (SEM) under secondary electron mode. Figure 2 shows the scanning electron micrographs of mine tailings at different magnifications. Table 2 shows the chemical compositions of these mine tailings extracted from x-ray fluorescence spectroscopy (XRF) technique.

EXPERIMENTAL METHODOLOGY

Details of Cement Mortar Mixes Developed

The study was fundamentally carried out with three varieties of cement mortar mixes. Cement mortar produced without any replacement of river sand was considered as reference mix, i.e., control mix (CM). The other two varieties of mortar mixes involve the replacement of river sand with mine tailings. The mortar mixes named with letter "I" belong to IOT-based mortar, and those with letter "C" belong to COT-based mortar. The subsequent numbers represent the replacement level by volume of river sand with mine tailings. All the mortar mixes developed in the study were prepared with water to cement ratio (w/c) of 0.45 and volume of binder to fine aggregate ratio of 1:3. The necessary moisture and water absorption corrections were incorporated while preparing the mortar mixes. The present study considers the guidelines given by IS 2250-1981 in selecting the required flow for mortar mixes.[35] To ensure better workability of produced mortar mixes for filling cavities, a minimum flow value of 150 mm was maintained throughout the study using superplasticizer. The selected range of flowability

FIG. 2

(*A*) Mine tailing, (*B*) scanning electron micrograph at ×500, and (*C*) scanning electron micrograph at ×10,000.

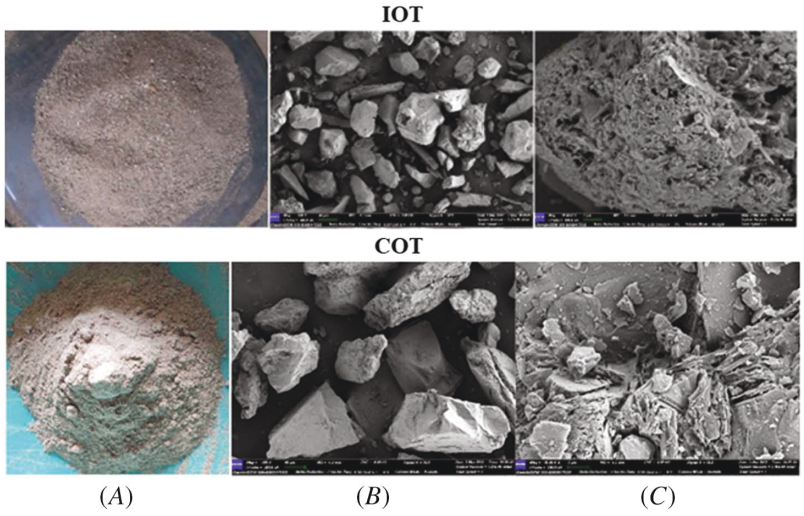

TABLE 2

Chemical compositions of IOT and COT

	% Mass							
Component	MgO	Al_2O_3	SiO_2	P_2O_5	SO_3	K_2O	CaO	MnO
IOT	1.12	4.54	39.50	0.09	0.09	0.21	0.70	0.31
COT	2.03	8.68	65.26	0.27	4.33	4.12	3.68	0.10
	% Mass							
Component	Fe_2O_3	Na_2O	Cl	TiO_2	CuO	SrO	ZrO_2	
IOT	53.43	…	…	…	…	…	…	
COT	9.65	0.69	0.01	0.64	0.39	0.06	0.07	

also satisfies the workability requirement under laboratory scale recommended by ASTM C270-08a, *Standard Specification for Mortar for Unit Masonry*.[36] The detailed mix proportion along with the basic properties of various mortar mixes produced in the present study are being tabulated in **Table 3**.

Production of Cement Mortar Samples

Cement mortar specimens of size 70.6 by 70.6 by 70.6 mm were cast and tested in the present investigation. Mixing of mortar was done in an automatic mortar mixer designed as per the guidelines mentioned in EN 196-1.[37] The cast specimens were further allowed to set under a humid environment (i.e., 27°C ± 2°C and 95 % relative humidity). Furthermore, these specimens were demolded after 24 h and immersed in normal potable water for curing maintained at 27°C ± 2°C till the date of testing. After the curing period of 3, 7, 28, 56, and 120 d, samples were taken out, dried, and tested to check their performance in the hardened state.

Details of Tests Performed

Fresh and Hardened Properties

The mortar mixes were assessed in the fresh state to check the workability and setting time. To investigate the hardened properties of produced mortars, tests were carried out using both destructive and nondestructive

TABLE 3
Details of the mortars produced

	Weight, kg/m^3					Dry Density, kg/m^3		Setting Time, min	
Mix Name	OPC	RS	IOT/COT	Water	SP, %	28 d	120 d	IST	FST
CM	777.50	1,943.25	…	349.88	0.00	2,247.82	2,273.40	333	448
				IOT-Based mortar					
I10	777.50	1,748.93	248.63	349.88	0.09	2,259.19	2,311.29	288	445
I20	777.50	1,554.60	497.25	349.88	0.10	2,324.55	2,385.17	283	439
I30	777.50	1,360.30	745.88	349.88	0.10	2,344.44	2,387.07	269	423
I40	777.50	1,165.95	994.50	349.88	0.25	2,356.00	2,389.34	227	412
I50	777.50	971.63	1,243.13	349.88	0.40	2,389.03	2,415.49	219	409
				COT-Based mortar					
C10	777.50	1,748.93	179.25	349.88	0.00	2,279.08	2,311.29	304	436
C20	777.50	1,554.60	358.50	349.88	0.10	2,200.00	2,239.30	302	426
C30	777.50	1,360.30	537.75	349.88	0.10	2,185.00	2,225.09	291	420
C40	777.50	1,165.95	717.00	349.88	0.10	2,119.95	2,224.52	275	404
C50	777.50	971.63	896.25	349.88	0.45	2,057.43	2,207.47	260	399

Note: FST = final setting time; IST = initial setting time.

methods. These tests were conducted at the age of 3, 7, 28, 56, and 120 d of curing for all mortar mixes. The average of three values obtained from three specimens was taken into consideration and the same was reported. Table 4 shows the details of the tests performed to assess the fresh and hardened properties.

Microstructural Analysis and Characterization Techniques Used

The performance of cement mortars was primarily influenced by their microstructure. Thus, understanding the microstructure of cement mortars and hydration products formed is very critical. The chunks were collected from the core of mortar samples after 28 and 120 d of curing and kept immersed in isopropyl alcohol for 24 h to discontinue the hydration mechanism beyond that specific curing age.[45,46] Furthermore, the chunks were dried in an oven at a temperature range of 40°C–60°C till the weight gets stabilized. These oven-dried samples were then stored in moist-free desiccators maintained using silica gel pellets and vacuum pump. These samples were

TABLE 4
Details of the tests conducted to investigate the fresh and hardened properties

Type	Test	Reference	Remarks
Fresh properties	Mini flow table test	BS EN 1015-3[38]	-Workability/flowability measurement-To fix the superplasticizer dosage required for maintaining a minimum flow diameter of 150 mm
	Setting time	ASTM C403/C403M-08[39]	-Initial and final setting time measurement using penetration resistance measurements
Hardened properties	Compressive strength	IS 4031-Part 6:1988[40]	-Using compressive testing machine at a loading rate of 35 MPa/min
	Dry density	BS EN 1015-10:1999[41]	-Oven-dried weight by volume method using weighing balance
	Permeable porosity	Safiuddin and Hearn[42] and Das, Singh, and Pandey[43]	-Vacuum water absorption technique using vacuum desiccators
	Water absorption	ASTM C948-81(2023)[44]	-Using change in weight at oven-dried condition and saturated surface–dried condition (immersed in water for not less than 24 h)

Note: BS EN 1015-3, *Methods of Test for Mortar for Masonry – Determination of Consistence of Fresh Mortar (by Flow Table)*; ASTM C403/C403M-08, *Standard Test Method for Time of Setting of Concrete Mixtures by Penetration Resistance* (Superseded); IS 4031-Part 6:1988, *Methods of Physical Tests For Hydraulic Cement-Part 6: Determination of Compressive Strength of Hydraulic Cement Other Than Masonry Cement (First Revision)*; BS EN 1015-10:1999, *Methods of Test for Mortar for Masonry - Determination of Dry Bulk Density of Hardened Mortar*; ASTM C948-81(2023), *Standard Test Method for Dry and Wet Bulk Density, Water Absorption, and Apparent Porosity of Thin Sections of Glass-Fiber Reinforced Concrete*.

examined using various characterization techniques to investigate the microstructure development in various types of cement mortars.

SEM and energy-dispersive x-ray spectroscopy—To investigate the developed microstructure and to carry out the morphological observations in optimized mortars (best performing), SEM technique was used in secondary electron mode. Furthermore, with the aid of energy-dispersive x-ray spectroscopy (EDS), the elemental composition of various types of cement mortars were analyzed. All the preserved samples were gold sputtered before taking them for microstructural examination.

XRD analysis—The mineralogical compositions of produced mortars were studied with the help of XRD studies. The preserved samples were ground and sieved in 75 μm IS sieve, and the collected powdered fine particles were taken for examination. The studies were carried out in Jeol-JPX 8P and Malvern Panalytical x-ray diffractometers equipped with Cu Kα radiation (40 kV/40 mA) at a scanning rate of 2°/min. The samples were examined with the 2θ angle ranging from 4° to 80°, and the received XRD patterns were further analyzed with the aid of software X'Pert High Score Plus.

Thermogravimetric analysis—Thermogravimetric analysis (TGA) was performed using RIGAKU TG-DTA 8112 analyzer to quantify the hydration products formed in different types of mortars at 28 and 120 d of curing age. The hardened paste from the preserved mortar samples were ground into powder and sieved through 75 μm sieve. The finer powder collected after sieving was characterized in a nitrogen purge environment at temperatures ranging from room temperature to 875°C. The heating rate was maintained at 20°C/min, and purge rate was maintained at 20 mL/min. When the hydrated mortar samples were subjected to elevated temperatures, thermogravimetric mass loss took place at various temperature boundaries because of the evaporation of free water, decomposition of hydration products by dehydration, dehydroxylation, and decarbonation.[45,47,48] These temperature boundaries were determined based on the endothermic peaks formed in derivative thermogravimetric curve (DTG) because of decomposition (weight loss) of compounds. The endothermic peak usually occurs in the temperature range of 50°C–120°C, 120°C–150°C, 110°C–300°C, and 230°C–380°C corresponding to the dehydration of water molecules from the ettringite, gypsum, CSH, and Friedel's salt, respectively.[45,49–54] Thereafter, the weight loss that occurs between 400°C and 500°C is associated with the decomposition of calcium hydroxide (CH).[45,50] Similarly, the temperature boundary associated with the decomposition of calcium carbonate appears in the temperature boundary of 600°C–800°C.[45]

Fourier transform infrared spectroscopy—Fourier transform infrared spectroscopy (FTIR) studies were performed with the aid of Bruker Alpha II FTIR equipment and OPUS software. The sample preparation is similar to that followed for XRD and TGA analysis. FTIR studies were performed to obtain the transmittance spectra in the wavelength ranges from 600 to 4,000 cm^{-1} under attenuated total reflectance (ATR) mode. The formation of different phases in cementitious system such as portlandite [$Ca(OH)_2$], C-S-H, calcium aluminum silicate hydrate (CASH), sulfates, and carbonate phases (such as ettringite, hemicarbonate, monosulfoaluminate, sulfoaluminate, calcium carbonate), etc., can be recorded based on the peak intensity and shift over the age of curing and also compared among the different types of mortars produced.

Analysis of Results and Discussions

PARTICLE PACKING OF PRODUCED CEMENT MORTAR MIXTURES

The particle packing of the 11 mortar mixes designed in the present study were analyzed using modified Andreasen and Andersen packing model.[55] To carry out the analysis, "EMMA" software was employed, which adopts the principle of a modified Andreasen and Andersen packing model. **Figure 3** shows the particle packing curves of mine tailing–based mortars. A distribution coefficient (q) of 0.30 appropriate for achieving medium workability was selected for the analysis.[45] From the obtained curves, it is clearly observable that the addition of mine tailings improves the particle packing of mortars till a specific replacement level by improving the extent of fitting to the target curve fixed by the modified Andreasen and Andersen packing model for highest particle

FIG. 3 Particle packing curves of (*A*) IOT-based mortars and (*B*) COT-based mortars determined using modified Andreasen and Andersen particle packing model.

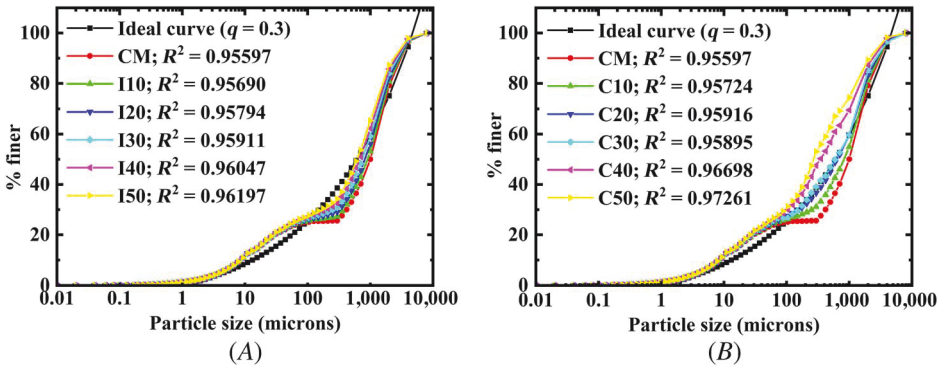

packing density.[56] Among the various mortar mixes designed, I20 and C30 mixes showed best fitting to the target curve.

FRESH PROPERTIES

Workability

Workability of different types of cement mortar mixes produced using varying dosages of IOT and COT as a replacement to river sand were checked using mini-flow table test. To ensure the desired workability in the produced mortar mixes, a minimum flow diameter of 150 mm was fixed and achieved with the aid of superplasticizer. The results reported in **figure 4*A*** (IOT-based mortar) and **figure 4*B*** (COT-based mortar) consist of flow diameter, flow value, and their corresponding dosage of superplasticizer consumption.

From the obtained results, it can be noticeable that the addition of IOT into the mortar mix as a replacement to river sand reduces the flow characteristics. This behavior can be clearly observed through the dosage of superplasticizer consumption with the percentage usage of IOT. The control mortar (CM) produced entirely with river sand as fine aggregate was observed to achieve required minimum flow diameter of 150 mm without consuming any superplasticizer. With the percentage usage of IOT as replacement to river sand, the flow characteristics were observed to become poorer because of the intrinsic properties of IOT. The rough textured IOT particles increase the friction between the particles, and the sharp edges of IOT particles block the movement of particles over one

FIG. 4 Flow characteristics of (*A*) IOT-based mortar and (*B*) COT-based mortar. Bwob = by weight of binder.

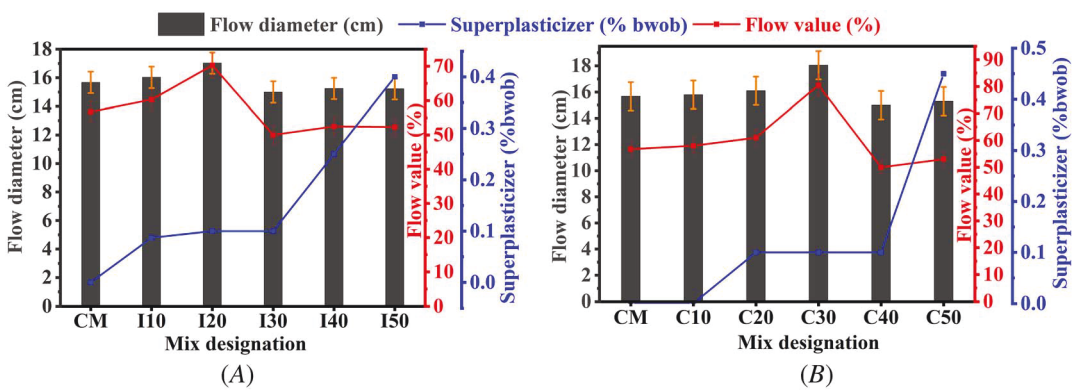

another. Also, the fine nature of IOT particles as compared with river sand leads to filling the void spaces and makes the mortar more uniform and cohesive till I20. Furthermore, a drastic fall in the flow values (i.e., from I30) was observed, which can be attributed to the poor gradational characteristics because of the occurrence of an excessive amount of fines, which demands higher water content for surface wetting, resulting in the formation of stiffer mortar mixes. These observations are in line with the inference made in some past studies.[19,20] The dry and harsh mortar mixes thus produced led to increased superplasticizer consumption to a greater extent, and thereby mortar mixes showed reduced workability.

Similarly, in the COT-based mortar, a sudden drop in the flow values was observed beyond 30 % replacement of river sand with COT because of the increased amount of fines in the mortar mix. This can be clearly observed through the flow values and the superplasticizer dosages consumed among the mixes C30, C40, and C50. Even though the superplasticizer dosage was kept constant between the mixes C30 and C40, a sudden declination in the flow values was observed, and further from C40 to C50 mix, a sudden increment in the superplasticizer dosage requirement was observed. However, the flow characteristics were found to be improved right from the CM till C30. This can be clearly noticeable from the flow values and their corresponding superplasticizer dosage from CM to C10 and C20 to C30 mix. This behavior can be attributed to the smooth glossy textured and angular-shaped COT particles that reduce the friction and help in movement among the particles with great ease.[25,26] Also, the fine particles of COT initially tend to fill the voids at lower replacement levels (till 30 %) and make the mixes uniform and cohesive, which helped in improving the flow characteristics.[15]

HARDENED PROPERTIES

Compressive Strength

Compressive strength development in control (CM), mine tailing–based mortars were measured at the curing ages of 3, 7, 28, 56, and 120 d, and the results are plotted as a histogram. **Figure 5*A*** and **5*B*** present the compressive strength of IOT-based and COT-based mortars, respectively.

The results obtained from both IOT and COT-based mortars exhibited a decreasing trend with the content of mine tailings in the initial days of curing (i.e., 3 and 7 d). Even though mine tailings accelerated the hydration reaction, leading to early setting of mortar (**Table 3**), they exhibited slightly lower compressive strength at early ages of curing till 7 d. This reduction in the compressive strength with the increasing amount of mine tailings is due to the slowing down of hydration reaction by the development of low permeability layer of heavy metals around the nonhydrated cement grains.[57,58] The presence of copper ions also slightly delays the hydration process because of the precipitation of oxides and hydroxides.[58–62]

However, a significant improvement in the compressive strength development of mine tailing–based mortars was observed with the progress in curing age (beyond 7 d of curing). This could be attributed to the acceleration in the hydration activity of cement particles under the influence of reactive minerals present in tailings. The presence of iron compounds at higher concentrations in the mortar accelerates the hydration process.[19,59,60,63,64] The additional calcium content added from the finer fractions of mine tailings also contributes in accelerating the hydration process.[59,60] The IOT-based mortars showed an increasing trend of compressive strength till a sand replacement level of 20 % and COT-based mortars till a sand replacement level of 30 %. The improved particle packing and thereby improvised particle packing density of the mortar mixes with the addition of IOT till 20 % and COT till 30 % helped the ingredients of mortar to undergo primary and possible secondary hydration reactions more effectually.[19,65] Because the mine tailings are rich in siliceous and aluminous compounds, the finer fractions of mine tailings facilitate in undergoing supplementary hydration reactions (secondary hydration reaction/pozzolanic reaction) after 7 d of curing, resulting in the formation of additional hydration products.[19]

The dry density results presented in **Table 3** also provide evidence for the occurrence of secondary hydration reaction. The difference between the dry densities of mine tailing–based mortars with the percentage replacement of sand was found to be reduced with the progress in curing age, which is attributed to the formation of additional hydration products by the finer fractions of tailings through secondary hydration reactions. These actions helped

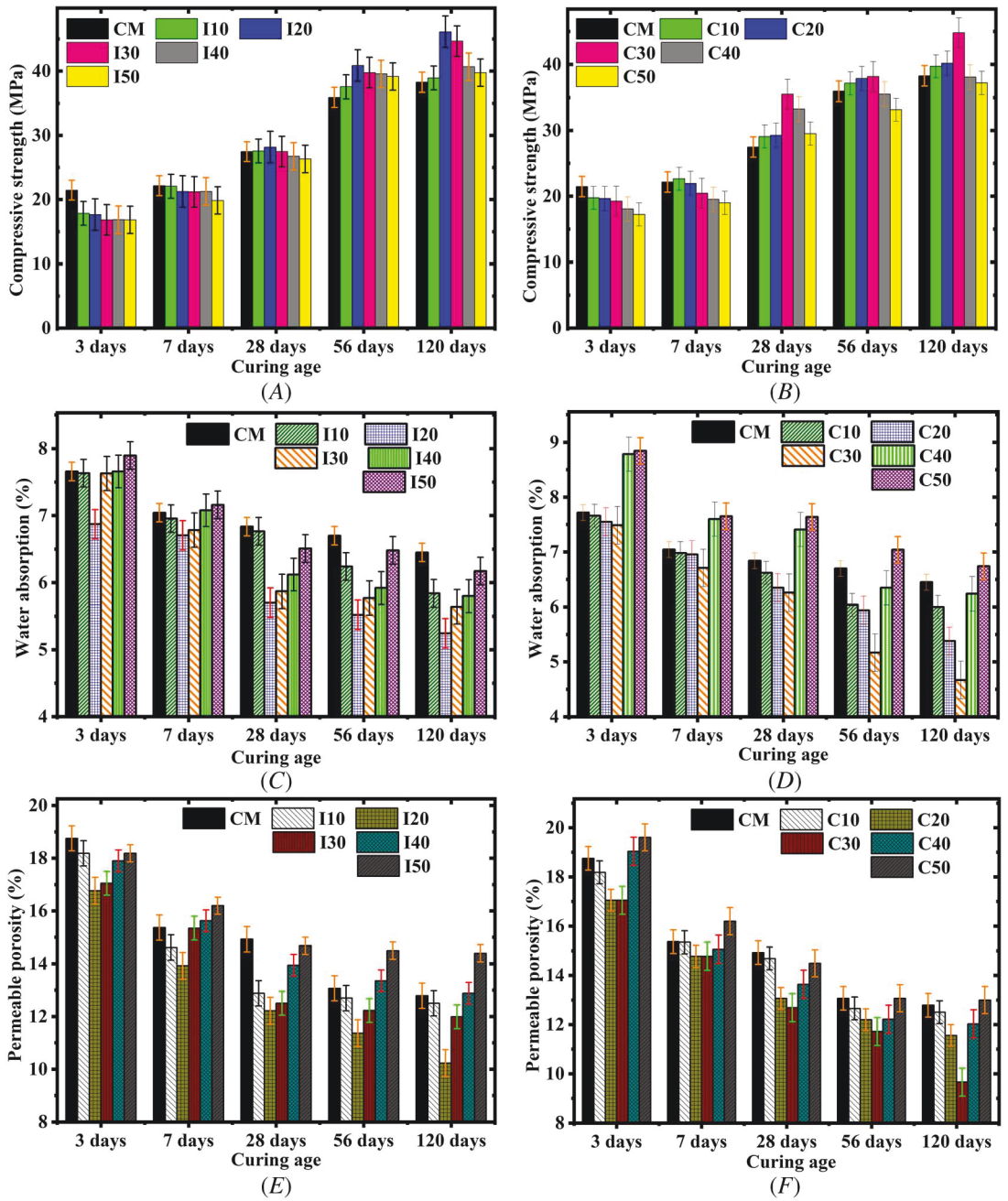

FIG. 5 (*A*) Compressive strength, (*C*) water absorption, and (*E*) permeable porosity of IOT-based mortars; (*B*) compressive strength, (*D*) water absorption, and (*F*) permeable porosity of COT-based mortars.

in refining the pore structure of mortars in an effective manner, leading to the formation of dense microstructure that enhances the hardened mechanical properties, such as compressive strength. It is also important to notice from the results that the compressive strength of the mortars reduces beyond the optimized dosage of mine tailings, which is due to the effect of poorer gradational characteristics and excessive silica-alumina content that restrains the degree of hydration reactions. A similar trend of compressive strength of mortar by the usage of IOT

and COT in relation to control mortar was observed in past literatures.[18–20,23–25] The percentage strength gain of I20 mortar was recorded to be 2.55, 13.75, and 20.53 % at the curing ages of 28, 56, and 120 d, respectively. Similarly, C30 mortar exhibits 29.17, 6.20, and 17.08 % at 28, 56, and 120 d of curing age, respectively.

Water Absorption and Permeable Porosity

The water absorption and permeable porosity of control and mine tailing–based mortars were assessed at the end of 3, 7, 28, 56, and 120 d of curing. Figure 5*C* and 5*D* presents the water absorption of IOT-based and COT-based mortars, respectively. Similarly, figure 5*E* and 5*F* represents the permeable porosity of IOT-based and COT-based mortars, respectively. The results obtained show that both water absorption and permeability porosity follow a quite similar trend with the percentage usage of mine tailings at all the curing ages. This could be due to the fact that the absorbed water predominantly accumulates in the permeable void spaces or pores present in the mortar mixes, and these pore volumes are usually regarded as porosity. It is also important to notice that both water absorption and permeable porosity reduce with the progress in curing age, which is due to the formation and accumulation of hydration products that refines the pore structure in mortar.

The utilization of mine tailings in the mortars as a replacement to river sand showed positive results in the case of water absorption and permeable porosity. The water absorption and permeable porosity were found to reduce with the increasing proportion of mine tailings till a certain replacement level and thereafter were found to increase. This behavior can be ascribed to the improved particle packing and improved affinity to undergo secondary hydration reaction by the finer fractions of mine tailings with the increasing level of sand replacement.[19,65] A similar trend of reducing water absorption with the usage of IOT was noticed in previous studies.[19] The mortar mixes "I20" and "C30" recorded the lowest water absorption and permeable porosity values. In addition to these, the lower water-absorbing capacity of IOT and COT in comparison with the river sand also contributes in reducing the water absorption and permeable porosity of mortar. However, exceeding the dosage of mine tailings beyond optimum percentage (i.e., 20 % of IOT and 30 % of COT) causes an increase in the water absorption and permeable porosity because of poor gradational characteristics and lack in water availability for undergoing hydration reactions caused by the increased amount of fines in the mortar mix. The reduced alkalinity in the mortar by the high-volume replacement of sand by mine tailings might also be the cause for the increased water absorption and permeable porosity.

MICROSTRUCTURE AND CHARACTERIZATION STUDIES

Mineralogical Characterization

The influence of different dosages of mine tailings on the mineralogical compounds was studied at the curing ages of 28 and 120 d using the XRD patterns. The XRD analysis was carried out for the control mortar and till one replacement level beyond the optimum mine tailing–based mortar (i.e., till I30 and C40). The details of the mineralogical compounds such as chemical name, empirical formula, and peak assignment designations are tabulated in Table 5.

Figure 6*A* presents the XRD patterns of 28 d cured and figure 6*B* those of 120 d cured mortar samples of the optimized mixes (i.e., CM, I20 and C30). By observing the XRD patterns of 28-d cured mortar samples, it is noticeable that the crystalline phases are greater and prominent in mine tailing–based mortars because of the presence of more CH and other unhydrated particles in comparison with the control mortar. The occurrence of portlandite (CH) peaks are greater and prominent in mine tailing–based mortars, which is due to additional portlandite formed from the calcium particles present in the finer fraction of mine tailings.[59,60] The increased portlandite peaks are also due to accelerated hydration reaction caused by improved particle-packing intensity and higher iron oxide compounds.[59,60,63–65] In addition to these, a preferential formation of additional calcium silicate hydrates (CSH) and CASH phases were observed because of the occurrence of effective primary and secondary hydration reactions facilitated by the finer fraction of mine tailings. The mineralogical compounds related to CSH and CASH phases such as gismondine, chabazite, xonotlite, and hillebrandite were found to be additionally formed.

TABLE 5

Details of the mineralogical compounds and their peak assignment

	Peak Assignment of COT-Based Mortar										Peak Assignment of IOT-Based Mortar					
	28 d Curing					120 d Curing					28 d Curing			120 d Curing		
Compound Details	CM	C10	C20	C30	C40	CM	C10	C20	C30	C40	I10	I20	I30	I10	I20	I30
Quartz (silicon oxide [SiO_2])	Q	Q	Q	Q	Q	Q	Q	Q	Q	Q	Q	Q	Q	Q	Q	Q
Portlandite (calcium hydroxide [$Ca(OH)_2$])	P	P	P	P	P	P	P	P	P	P	P	P	P	P	P	P
Hillebrandite (calcium silicate hydroxide [$Ca_2(SiO_3)(OH)_2$])			2		2								2			2
Kamaishilite (calcium aluminum silicate hydroxide [$Ca_2Al_2SiO_6(OH)_2$])		3				3					3	3				
Tobermorite (calcium silicate hydroxide hydrate [$Ca_5(OH)_2Si_6O_{16}{\cdot}4H_2O$])	T														T	
Xonotlite (calcium silicate hydrate [$Ca_6Si_6O_{17}(OH)_2$])			X		X	X	X			X	X	X		X	X	
Calcium silicate hydrate ($Ca_2SiO_4{\cdot}H_2O$)			5				5	5	5							
Chabazite (CASH [$Ca_2Al_4Si_8O_{24}{\cdot}12H_2O$])				6	6				6						6	
Wairakite (CASH [$CaAl_2Si_4O_{12}{\cdot}2H_2O$])	W			W					W			W			W	
Gismondine (CASH [$CaAl_2Si_2O_8{\cdot}4H_2O$])		7	7				7	7		7	7		7	7		7
Calcite (calcium carbonate [$CaCO_3$])	C	C	C	C	C	C	C	C	C	C	C		C	C		C
Gypsum (calcium sulfate hydrate [$CaSO_4{\cdot}2H_2O$])	G			G	G	G	G	G	G		G	G	G		G	
Ye'elimite (calcium aluminum oxide sulfate [$Ca_3Al_6\ O_{12}{\cdot}CaSO_4$])	Y			Y					Y	Y		Y		Y	Y	

FIG. 6

XRD pattern of optimized mortars at the curing ages of (*A*) 28 d and (*B*) 120 d.

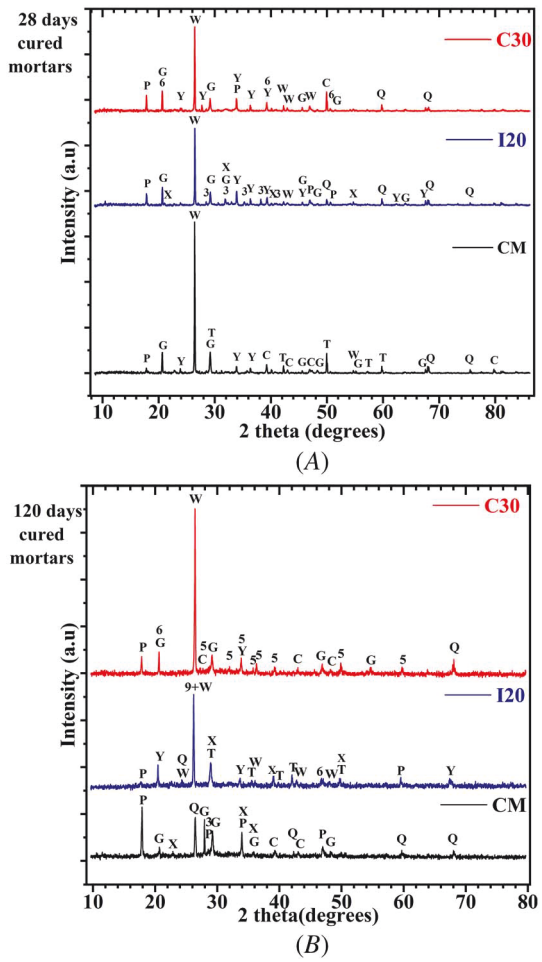

However, by observing the XRD patterns of 120 d–cured mortar samples, it can be noticed that the XRD patterns of mine tailing–based mortars appeared more amorphous than 28 d ones and also in comparison with the control mortar. This is attributed to the effective conversion of crystalline CH to amorphous gel-like structure formed by CSH and CASH phases through primary and secondary hydration reactions. The produced CH in control mortar remained mostly unutilized after 28 d of curing. However, the portlandite produced in the mine tailing–based mortars appeared to get consumed for secondary hydration reactions. The formation of additional hydration phases related to CSH and CASH are evident for the consumption of portlandite in mine tailing–based mortars. The mineralogical compounds related to CSH and CASH phases such as gismondine, chabazite, wairakite, hillebrandite, and tobermorite were found to be additionally formed, which helped in refining the pore structure of mine tailing–based cement mortar. In addition, the occurrence of various phases of carbonates, gypsum, and ettringites are also the cause for more crystalline XRD patterns in control mortar.

Overall, by observing the XRD patterns, there can be seen that more mineralogical compounds related to calcium silicates and calcium aluminum silicates were formed with fewer carbonates, gypsum, and ettringite phases by the utilization of mine tailings in cement mortar. This development in mine tailing mortars helped to perform superior compared with control mortar. This enhanced performance can also be witnessed through the measured engineering properties such as compressive strength, water absorption, and permeable porosity.

FIG. 7 TG and DTG curves of (*A*) IOT-based mortar after 28 d of curing, (*B*) IOT-based mortar after 120 d of curing, (*C*) COT-based mortar after 28 d of curing, and (*D*) COT-based mortar after 120 d of curing.

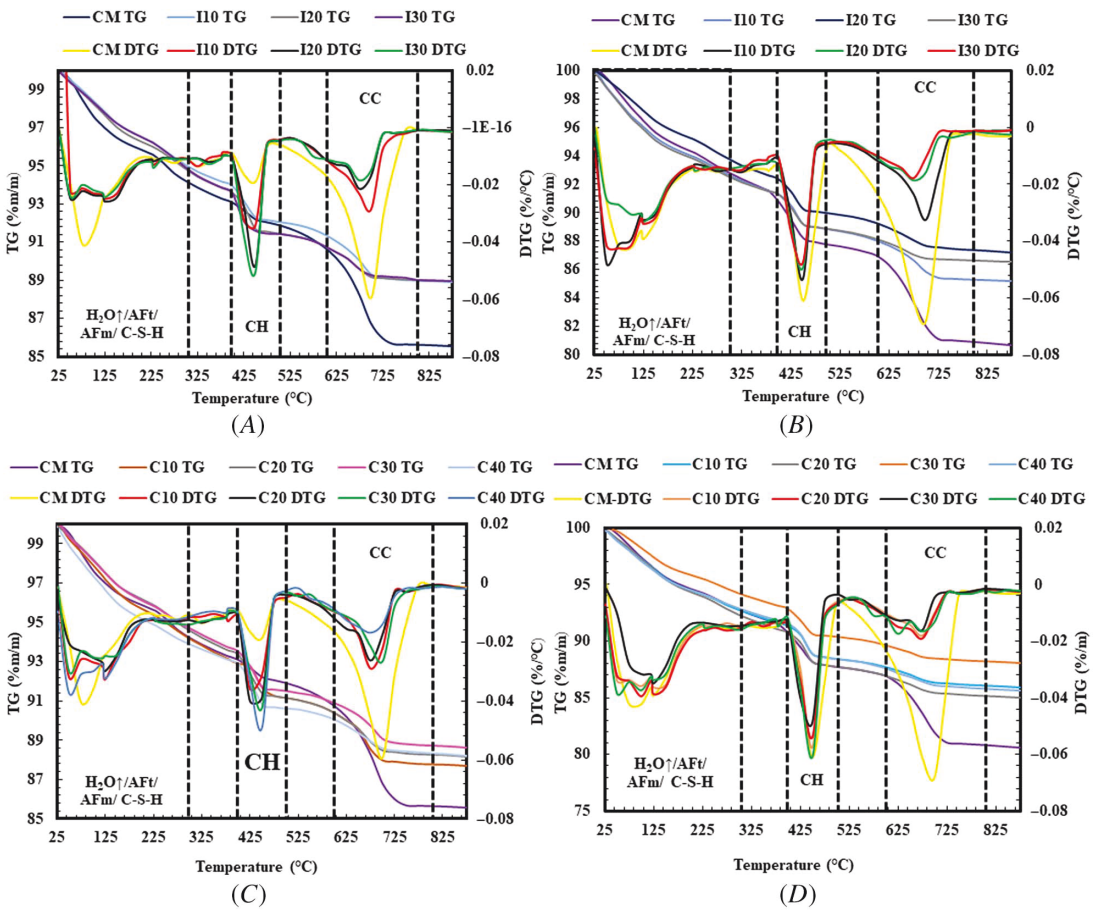

TGA on IOT and COT-Based Cement Mortar

From the thermogravimetric analyzer, the weight loss of the mortar samples with the increasing temperature was recorded, and for the analysis, Thermogravimetric (TG)/Derivative Thermogravimetric (DTG) curves were plotted. **Figure 7*A*** and ***7B*** presents the TG/DTG curves of 28 and 120 d cured IOT-based mortar samples, respectively. Similarly, **figure 7*C*** and ***7D*** shows the TG/DTG curves of 28 and 120 d cured COT-based mortar samples, respectively.

In the present study, the hydration products such as calcium hydroxide (CH) and calcium carbonate (CC) were quantified on the basis of their decomposition by weight loss at their specific temperature boundaries. The various other hydration products such as gypsum, ettringite, CSH, CASH, Friedel's salts, etc., were not computed in the present study because of the overlap among the respective temperature boundaries.[45,51,52] The quantified values of CH and CC are graphically represented in **figure 8**.

The TGA results of 28 d cured IOT and COT–based mortar samples show increasing CH content with the increasing percentage of river sand replacement by mine tailings. This is attributed to the accelerated hydration reaction because of enhanced particle packing density and participation of elements of iron, i.e., Fe^{+} generated from the finer fractions of mine tailings.[19,59,60,63,64] In addition to this, the additional calcium oxide added from the mine tailings also marginally contributes to the generation of CH.[59,60] Meanwhile, there will be some influence

FIG. 8

Phase compounds formed in IOT-based mortar [(*A*) CH; (*C*) CC] and COT-based mortar [(*B*) CH; (*D*) CC] after 28 and 120 d of curing.

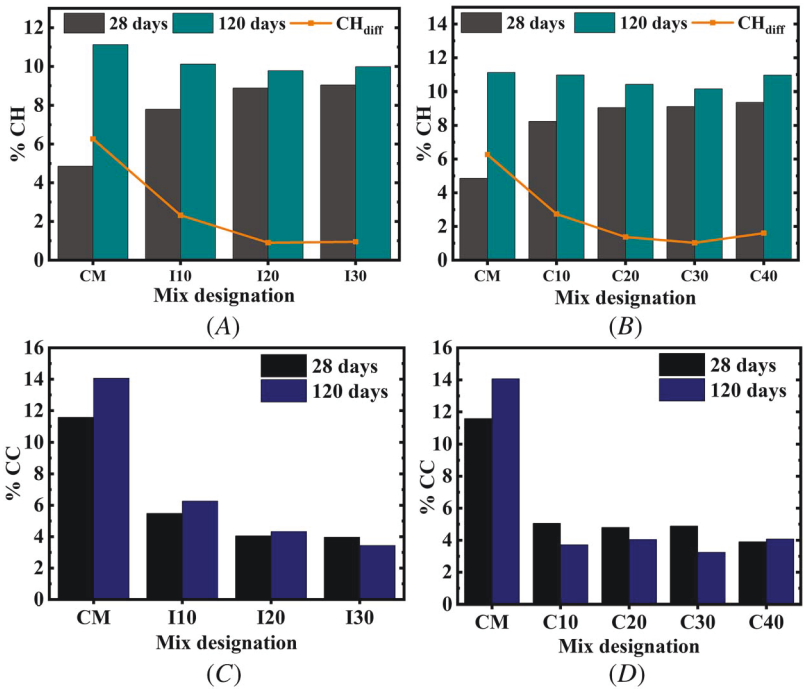

of heavy metals and copper ions too. The heavy metals present in mine tailings create a low permeability layer around the particles, which delays the hydration reaction.[57,58] The presence of copper ions also slightly delays the hydration process because of the precipitation of oxides and hydroxides.[58–62] The delayed hydration reaction thus slows down the consumption of CH for further reactions, which creates a higher CH reserve in the mine tailing–based mortars pore solution. The improved particle packing caused by the finer PSD of mine tailings also leads to the extensive formation of CSH/CASH gels along with a higher volume of portlandite.[59,60,63–65]

Apart from these, mine tailing–based mortars recorded lower content of CC, which can be seen in **figure 8**, where the control mortar showed the highest amount of CC. It is also essential to notice that there is a preferential formation of ettringite in the control mortar, which can be seen by an intensive endothermic peak in the DTG curve. However, the mine tailing-based mortar showed a comparatively wider but less intense endothermic peak, which is evident for the lesser formation of gypsum and ettringite.

By observing the DTG curves and quantified CH values corresponding to 120 d cured samples, it can be seen that the generation of CH continues with the curing age in all types of mortars. However, the consumption of CH for the secondary hydration reactions was found to be significantly greater in mine tailing–based mortars, which can be seen from the reducing trend of CH_{diff} (difference between the CH values at 28 and 120 d curing) shown in **figure 8**. Conversely, the endothermic peaks corresponding to CSH and CASH were found to be broadened and intensified with the curing age, which signifies the effective formation of CSH and CASH gels in mine tailing–based mortars. It is also important to note that the consumption of CH is slightly greater in the optimized mine tailing–based mortar (i.e., I20 and C30), which is due to the optimized mine tailing percentage favorable for undergoing reactions and superior particle packing that might helped in undergoing the reactions efficiently. However, the observed values of CH fall in the reported range of CH content (2.5 to 14.5 %) in previous findings of cementitious mortar/concrete.[66–69] However, the CH content in cementitious paste lies in the higher range of about 7 to 32 % because of effective hydration reactions facilitated by cement grains and water.[45,52,70,71] The quantified values of CC by the end of 120 d of curing also shows the presence of CC in lower volume in mine

tailing-based mortars. Thus, the additionally formed CSH/CASH gels along with the lower content of CC, ettringite and gypsum ensures better performance in the case of mine tailing-based mortars.

FTIR

Figure 9*A* and 9*B* illustrates the FTIR spectra of IOT-based cement mortar at the curing ages of 28 and 120 d, respectively. Similarly, figure 10*A* and 10*B* illustrates the FTIR spectra of COT-based cement mortar at the curing ages of 28 and 120 d, respectively. The corresponding details about the functional group assignment for various wavenumbers are presented in Table 6.

It can be observed from the FTIR spectra that the vibration bands and corresponding functional groups assigned were found to be the same in all types of mortars (i.e., CM, IOT-based and COT-based mortar) both at 28 and 120 d of curing. By observing the FTIR spectra, it can be noticed that the vibration band corresponding to Si-O-Si asymmetric stretching found in the wavenumber range of 1,000 cm^{-1} is more prominent in control mortar and optimized mine tailing mortars (i.e., I20 and C30). These vibration bands were found to be more intense and broader than the rest of the mine tailing–based mortars.[72–74] This could be attributed to the uninterrupted hydration reactions that occurred in CM and effective hydration reactions that took place under the effect of superior particle packing along with the presence of iron oxide mine tailings, which facilitated the generation of a higher amount of CSH gels.[65] The occurrence of secondary hydration reactions facilitated by the finer fractions of mine tailings also generates additional C-S-H phases.

FIG. 9 FTIR spectra of control and IOT-based mortar samples at (*A*) 28 d of curing and (*B*) 120 d of curing.

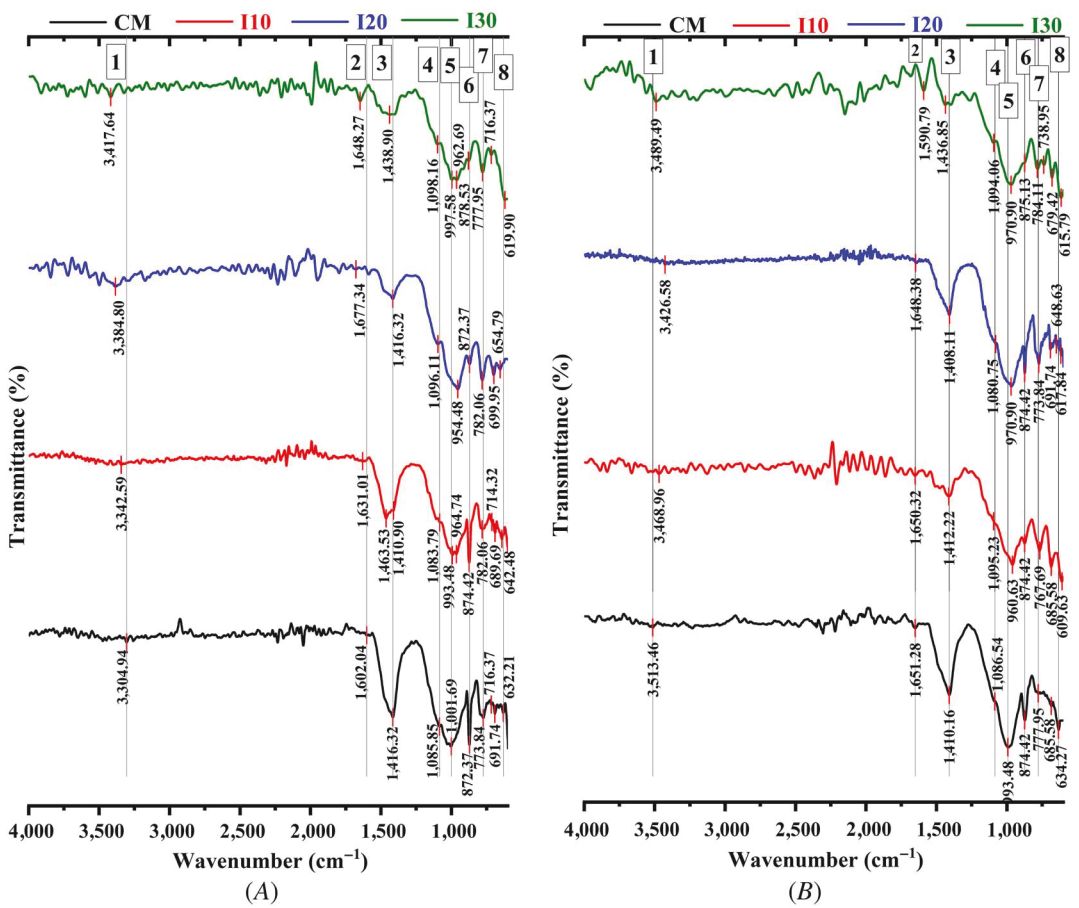

FIG. 10 FTIR spectra of control and COT-based mortar samples at (*A*) 28 d of curing and (*B*) 120 d of curing.

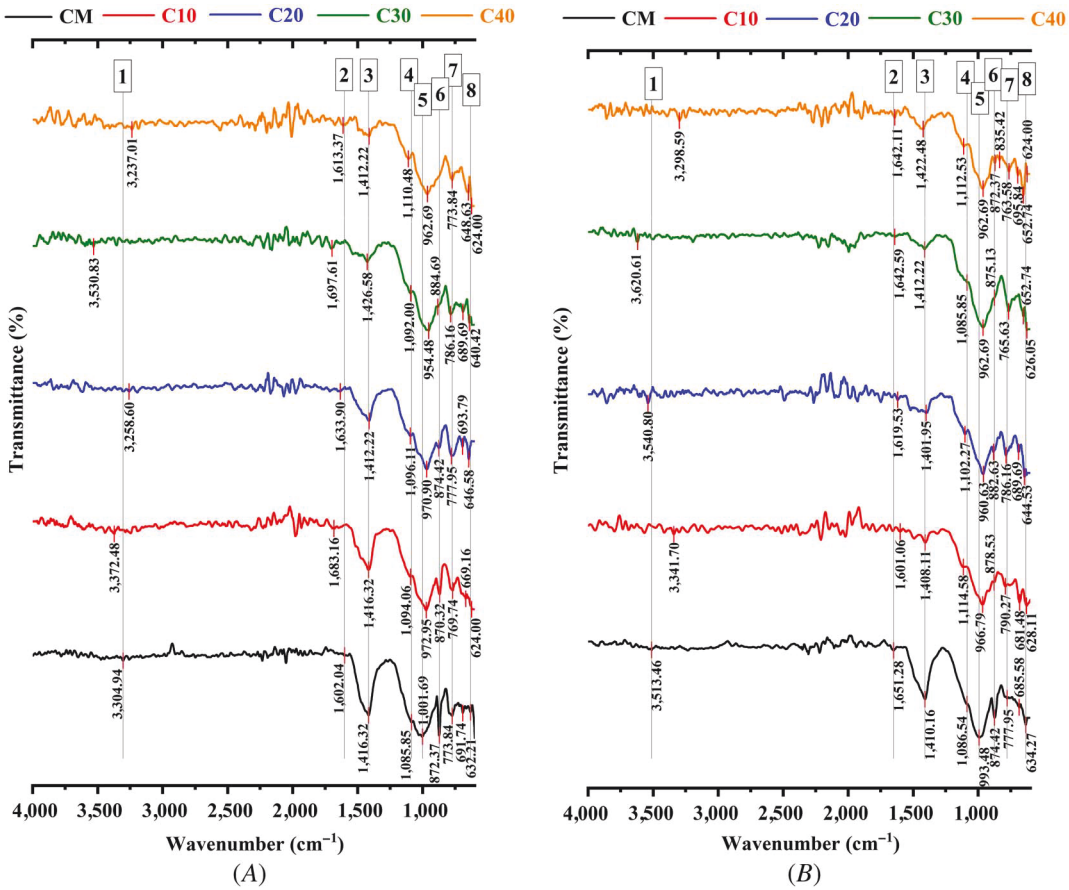

For brevity, the wavenumbers corresponding to Si-O-Si/Al asymmetric stretching are represented using grayscale shading technique Table 6. The grayscale shading of the table cells diverges from black (dark) to white (bright), indicating the variation of wavenumber from maximum value to minimum value, respectively. By observing the wavenumbers corresponding to Si-O-Si/Al asymmetric stretching band, a change in grayscale shading from black to white, by the utilization of mine tailings can be observed. This variation signifies the decrease in wavenumbers from 1,001.68 to 954.48 cm^{-1} in 28 d cured mortars and from 993.48 to 960.63 cm^{-1} in 120 d cured mortars. The decrease in wavenumber of Si-O-Si/Al asymmetric stretching band signifies the change of microstructure followed by the formation of more amorphous products with stronger bonds because of the additional formations of silicates and aluminosilicate hydrates.[66,75–77] It is also important to note that the I10 and I30 mortars showed additional peaks at wavenumbers 993.48 and 997.58 cm^{-1}, respectively, which is evident for the formation of additional C-S-H phases by the intrusion of IOT in mortar.

The vibration band associated to Si-O-Si/Al symmetric stretching were found to be more prominent in mine tailing-based mortars both at 28 and 120 d of curing. Especially in the case of 120 d cured samples, the vibration bands corresponding to Si-O-Si/Al symmetric stretching were found to be comparatively broader and more intense than that of control mortar. This is mainly ascribed to the formation of additional CSH and CASH phases through the effective hydration reactions facilitated by the improved particle packing achieved from the fine nature of mine tailings.[65] The finer fractions of mine tailings also contribute in the additional formation of CSH and CASH gels through secondary hydration reactions. The additional peak found at the wavenumber

TABLE 6

Details of the functional group assignment at different wavenumbers

Notation Number	Age of Curing	Wavenumber (cm ^{1}) Corresponding to Different Peaks								Functional Group Assignment
		CM	I10	I20	I30	C10	C20	C30	C40	
1	28	3,305	3,343	3,385	3,418	3,372	3,259	3,531	3,237	O-H asymmetric stretching (Due to bonded water in portlandite and free water)
	120	3,513	3,469	3,427	3,489	3,342	3,541	3,621	3,299	
2	28	1,602	1,631	1,677	1,648	1,683	1,634	1,698	1,613	O-H asymmetric bending (Due to free water)
	120	1,651	1,650	1,648	1,591	1,601	1,620	1,643	1,642	
3	28	1,416	1,464	1,416	1,439	1,416	1,412	1,427	1,412	O-C-O asymmetric stretching (Due to carbonates)
	120	1,410	1,412	1,408	1,437	1,408	1,401	1,412	1,422	
4	28	1,086	1,084	1,096	1,098	1,094	1,096	1,092	1,110	S-O stretching (Due to gypsum and ettringites)
	120	1,087	1,095	1,081	1,094	1,115	1,102	1,086	1,113	
5	28	…	993	…	998	…	…	…	…	Si-O-Si/Al asymmetric stretching (Due to silicates and aluminosilicate hydrates)
		1,002	965	954	963	973	971	954	963	
	120	993	961	971	971	967	961	963	963	
6	28	872	874	872	879	870	874	885	…	O-C-O bending (Due to carbonates)
	120	874	874	874	875	879	883	875	872	
7	28	774	782	782	778	770	778	786	774	Si-O-Si/Al symmetric stretch (Due to silicates and aluminosilicate hydrates)
		716	714	…	716	…	…	…	…	
		692	689	699	…	…	693	689	…	
	120	778	767	773	784	790	786	765	763	
		…	…	…	738	…	…	…	…	
		686	685	691	679	681	689	…	695	
8	28	632	642	655	620	669	647	640	649	S-O bending (Due to gypsum and ettringites)
		…	…	…	…	624	…	…	624	
	120	634	610	618	616	628	645	653	653	
		…	…	…	…	…	…	626	624	

738.95 cm^{-1} could be due to the formation of additional C-S-H/CASH phases by the intrusion of IOT in mortar. All these observations are found to be in good alignment with the XRD analysis data.

By observing the recorded wavenumbers, a considerable shift of Si-O-Si/Al symmetric stretching bands toward the lower wavenumber by the inclusion of mine tailings. This fact expresses that stronger bonds were developed by the formation of additional CSH and CASH phases in mine tailing–based mortars.[66,75–77] It is also important to notice that there is no significant shift observed in the wavenumbers associated with the Si-O-Si/Al symmetric stretching by the inclusion of mine tailing by the end of 28 d of curing. This could be due to the negligible amount or absence of secondary hydration reactions at the early stages of curing by the delayed hydration activity caused by the heavy metals.[57,58]

However, a drastic reduction in the intensities of vibration bands corresponding to O-C-O asymmetric stretching and O-C-O bending with the usage of mine tailings was observed in both 28 and 120 d cured mortar

FIG. 11 Scanning electron micrograph of (*A*,*B*) control (CM), (*C*,*D*) I20, and (*E*,*F*) C30 mortar at 28 d of curing.

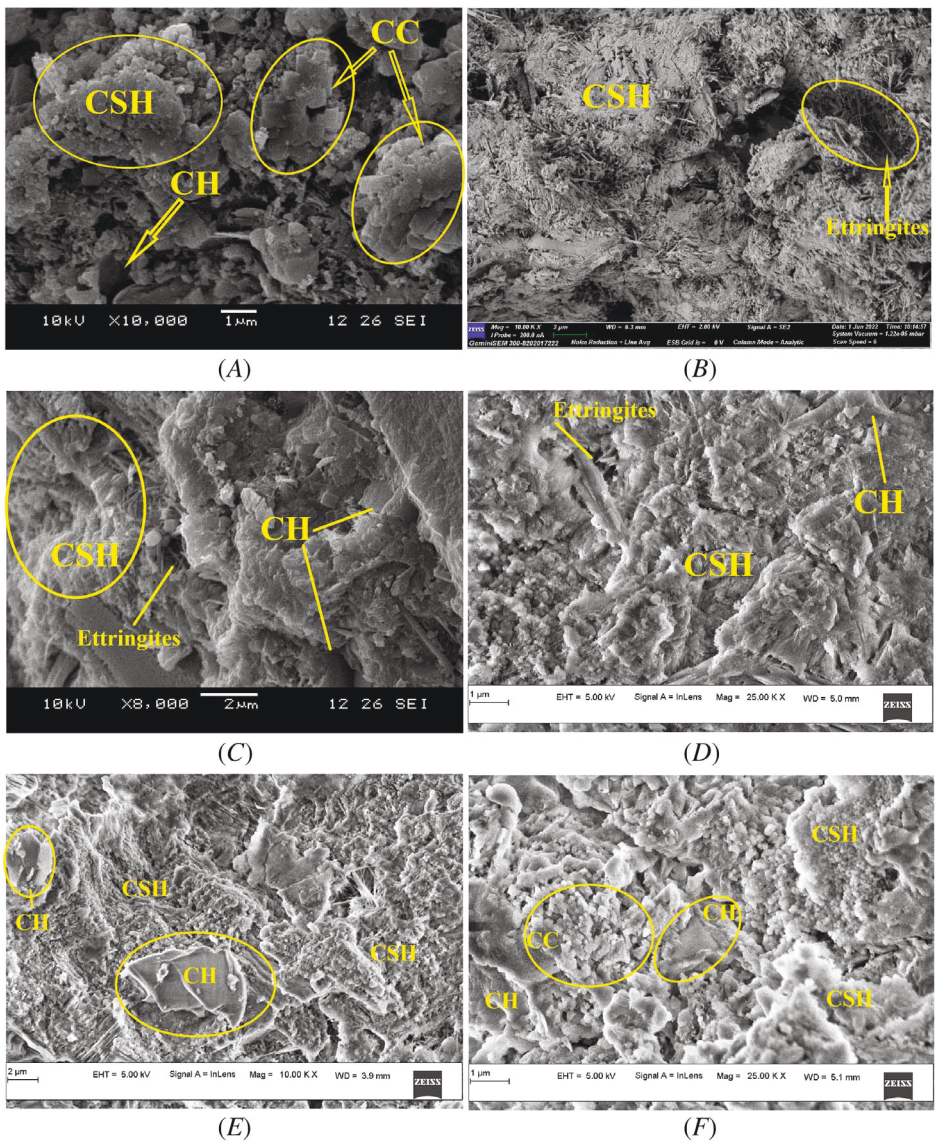

samples. This behavior is attributed to the increased compactness in the mine tailing–based mortars owing to accelerated hydration activity that leads to the formation of additional CSH and CASH gels, which acts as carbonation barrier.[78] This feature helped the mine tailing–based mortars to have an advanced quality microstructure even though the hydration reactions lagged in the early stages of curing. These observations are in good alignment with the TGA and SEM studies.

SEM and EDS

The morphology and microstructure of hydrated samples of control, optimized IOT, and COT mortars (i.e., CM, I20 and C30) were studied using SEM at the curing ages of 28 and 120 d. **Figures 11** and **12** depict the scanning

FIG. 12 Scanning electron micrograph of (*A*,*B*) control (CM), (*C*,*D*) I20, and (*E*,*F*) C30 mortar at 120 d of curing.

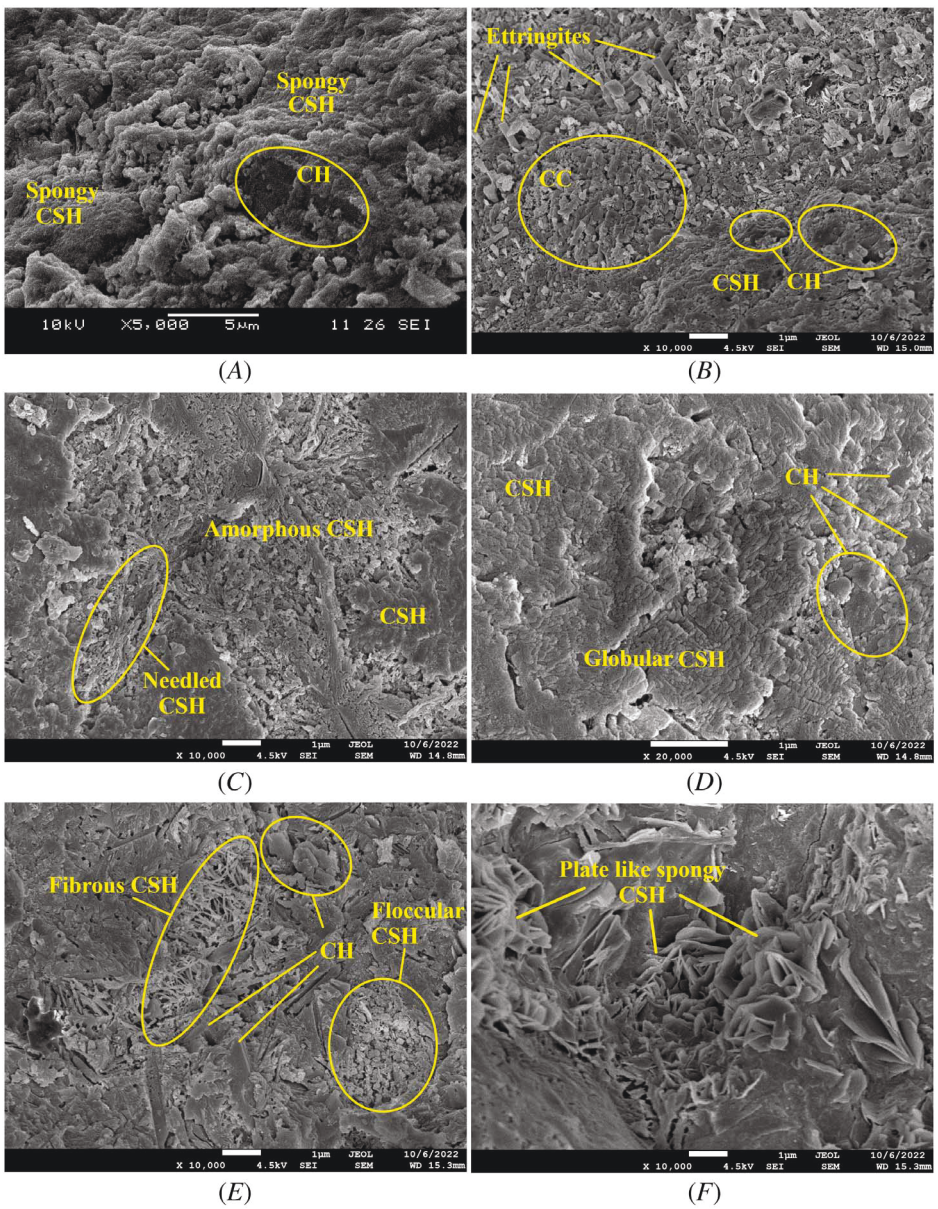

electron micrographs of 28 and 120 d cured mortar samples, respectively. The compounds in the micrographs were visually identified based on their morphological structure.[79] Gray pentagonal/hexagonal/irregular plate-shaped structures with smooth texture indicate calcium hydroxide crystals.[80,81] Gray areas having amorphous/globular/spongy/fibrous/granular/foil-like/sheet-like/cloud-like/grid-like structure with short needles and fine bundles represent calcium silicate hydrate.[80,81] Colorless to yellowish-white needle-like clusters of rod-shaped ettringite crystals mostly occur in the lining of voids or cracks and are considered as ettringites.[80,81] Calcite crystals generally appear as elongated/rhombohedral (diamond-shaped)/cubic box-shaped/walnut-shaped structure with well-defined facets looks granular and clustered together in a loosely packed structure, yielding rough surfaces.[82,83]

Furthermore, the elemental composition of these mortar samples was investigated using area method in EDS technique. The calcium/silicate atomic ratio was calculated from the obtained results and tabulated in **Table 7**. It was used to examine the extent of formation of major products related to hydration, such as calcium hydroxide (CH) and CSH. Numerous studies have claimed that the formation of CSH the through hydration process highly depends on the calcium and silicate ions present in the pore solution.[79,84,85] It has been reported that the cement matrix having a lower calcium/silicate atomic ratio signifies a dense microstructure owing to the formation of a strongly built CSH network.[86,87]

By observing the SEM micrographs of 28 d cured samples, it is possible to notice that the mine tailings–based mortars developed additional portlandite, CSH, and CASH phases from the accelerated hydration reactions facilitated by the superior particle packing and added calcium oxide and iron oxide compounds from the finer fractions of mine tailings.[59,60,63,64] The increased calcium/silicate ratio in mine tailing-based mortars is evident for the increased formation of portlandite. However, the extensive formation of CSH and CASH phases in mine tailing-based mortars helped in achieving a quality microstructure that is responsible for the improved hardened properties.

Similar kind of observations can also be made in 120 d cured mortar. However, the scanning electron micrographs were found to have much more CSH and CASH phases because of the succession of hydration reactions with the curing age. As depicted in the SEM micrographs, the iron ore tailing–based mortar showed globular, needle-like, and amorphous network of CSH and CASH phases. However, floccular, fibrous, and plate-like

TABLE 7
EDS elemental analysis of control, IOT-based, and COT-based mortars after a curing period of 28 and 120 d

	Atomic Weight (%) of 28 d Cured Mortar			Atomic Weight (%) of 120 d Cured Mortar		
Element	CM	I20	C30	CM	I20	C30
C	15.43	14.04	15.38	10.00	12.05	17.05
Ca	21.20	20.97	20.96	9.85	15.70	10.90
O	54.79	55.69	55.48	60.60	50.90	51.05
Al	0.22	0.75	0.81	2.55	0.95	3.40
Si	7.475	6.9	6.28	4.05	6.60	5.50
Mg	0.16	0.14	0.18	…	0.25	0.05
S	0.28	0.28	0.28	10.65	3.35	0.75
Cl	0.03	0.05	0.02	…	…	…
K	0.11	0.08	0.13	0.30	0.60	1.80
Fe	0.3	1.1	0.48	1.75	1.55	0.10
Na	…	…	0.21	0.25	0.05	0.65
P	…	…	…	…	3.10	…
Mn	…	…	…	…	4.80	1.45
Ti	…	…	…	…	…	0.30
Zr	…	…	…	…	…	1.45
Ca/Si	2.83675	3.03913	3.33758	2.432	2.378	1.98198

structured CSH and CASH phases were formed in COT base mortars. These diversely formed CSH and CASH phases beyond 28 d of curing in the mine tailing-based mortars are evident for the formation of additional hydration products through secondary hydration reactions, facilitated by the reactive finer fractions present in mine tailings. The reduction in calcium/silicate atomic ratio in mine tailings mortar at the end of 120 d curing was also significantly higher than control mortar because of the effective utilization of CH for secondary hydration reactions. It is also important to notice that the occurrence of higher volume of CC and ettringites can also be observed only in the SEM images of control mortar. However, the mine tailing-based mortars illustrate less CC and ettringites with ample amounts of CSH and CASH.

Thus, the additional hydration products formed from the primary and secondary hydration reactions help in densifying the mortar microstructure, which steers the mine tailings-based mortars to perform better than conventional mortar.

Conclusions

After analyzing the experimental results in detail, the following conclusions can be drawn:

- The preliminary investigations on the mine tailings used in the present study revealed that they have comparable properties with river sand and hence could be used as an alternative to river sand in developing cementitious composites.
- The fresh properties, such as workability and setting time, reduce with the inclusion of mine tailings as a replacement to river sand. The present study confirms the requirement of superplasticizer and recommends desired volumes of superplasticizer (about 0–0.45 % by weight of binder) for achieving the required flow of 150 mm in different mortar mixes.
- The improved particle packing by the inclusion of mine tailings till certain replacement level of river sand helped in improving the hardened properties of mortar such as compressive strength, water absorption, and permeable porosity. However, the dry density of mortars greatly relies on the specific gravity of tailings used.
- The outcome from the characterization studies, such as lowering of calcium/silicate ratio in EDS, formation of additional CSH, and CASH peaks in XRD, increased consumption of CH observed in TGA and occurrence of broad, intensive Si-O-Si/Al stretching bands with considerable shifts toward lower wavenumber in FTIR studies confirms the occurrence of secondary hydration reactions by the finer fractions of mine tailings which helped in improving the microstructure (can be observed through SEM images) and overall performance (compressive strength, water absorption, and permeable porosity) of the cement mortar.
- The study concludes that 20 % of IOT and 30 % of COT by volume of river sand can be considered as a potential replacement level for achieving superior performance in cement mortar.
- By the end of 120 d of curing, I20 showed 20.53 % higher compressive strength, 4.92 % higher dry density, 1.20 % lower water absorption, and 2.56 % lower permeable porosity than the control mortar. Similarly, C30 showed 17.08 % higher compressive strength, 2.17 % lower dry density, 1.78 % lower water absorption, and 3.13 % lower permeable porosity.
- The fineness of the material and angular particle shape along with the presence of higher concentration of silica and alumina in the finer fractions of COT played a key role in achieving the higher level of replacement for copper ore tailings in comparison with iron ore tailings.
- The rough textured fine particles of IOT along with higher concentration of Fe_2O_3 helped in achieving higher density and better performance in iron ore tailing–based mortar.

References

1. J. R. Owen, D. Kemp, É. Lèbre, K. Svobodova, and G. Pérez Murillo, "Catastrophic Tailings Dam Failures and Disaster Risk Disclosure," *International Journal of Disaster Risk Reduction* 42 (January 2020): 101361, https://doi.org/10.1016/j.ijdrr.2019.101361

2. F. F. Carmo, A. O. Lanchotti, and L. H. Y. Kamino, "Mining Waste Challenges: Environmental Risks of Gigatons of Mud, Dust and Sediment in Megadiverse Regions in Brazil," *Sustainability* 12, no. 20 (October 2020): 8466, https://doi.org/10.3390/su12208466
3. W. Pytel, "Risk Assessment of Mine Tailings/Waste Surface Ponds," in *Mine Waste 2010: Proceedings of the First International Seminar on the Reduction of Risk in the Management of Tailings and Mine Waste* (Perth, Australia: Australian Centre for Geomechanics, 2010), 229–242, https://doi.org/10.36487/ACG_rep/1008_20_Pytel
4. Z. Różański, "Fire Hazard in Coal Waste Dumps–Selected Aspects of the Environmental Impact," *IOP Conference Series: Earth and Environmental Science* 174 (2018): 012013, https://doi.org/10.1088/1755-1315/174/1/012013
5. C. Cacciuttolo, D. Cano, and M. Custodio, "Socio-environmental Risks Linked with Mine Tailings Chemical Composition: Promoting Responsible and Safe Mine Tailings Management Considering Copper and Gold Mining Experiences from Chile and Peru," *Toxics* 11, no. 5 (May 2023): 462, https://doi.org/10.3390/toxics11050462
6. D. P. Mohapatra and D. M. Kirpalani, "Process Effluents and Mine Tailings: Sources, Effects and Management and Role of Nanotechnology," *Nanotechnology for Environmental Engineering* 2, no. 1 (December 2016): 1, https://doi.org/10.1007/s41204-016-0011-6
7. C. Falagán, B. M. Grail, and D. B. Johnson, "New Approaches for Extracting and Recovering Metals from Mine Tailings," *Minerals Engineering* 106 (May 2017): 71–78, https://doi.org/10.1016/j.mineng.2016.10.008
8. H. R. Watling, "Review of Biohydrometallurgical Metals Extraction from Polymetallic Mineral Resources," *Minerals* 5, no. 1 (March 2015): 1–60, https://doi.org/10.3390/min5010001
9. Ministry of Mines, "Report of the Working Group on Mineral Exploration & Development (Other than Coal and Lignite) for the Twelfth Five Year Plan," India Environmental Portal, 2011, https://perma.cc/4N5J-GZBH
10. Indian Bureau of Mines, "Part-I: General Reviews," in *Indian Mineral Yearbook 2022* (Nagpur, India: Ministry of Mines-Government of India, 2023), 1–35, https://web.archive.org/web/20231019084143/https://ibm.gov.in/IBMPortal/pages/indian-minerals-yearbook–2022-vol–i–general-reviews-
11. C. Sudha, A. K. Kottuppillil, P. T. Ravichandran, and K. Divya Krishnan, "Study on Mechanical Properties of Concrete with Manufactured Sand and Bagasse Ash," *Indian Journal of Science and Technology* 9, no. 34 (2016): 1–5, https://doi.org/10.17485/ijst/2016/v9i34/95867
12. M. Pilegis, D. Gardner, and R. Lark, "An Investigation into the Use of Manufactured Sand as a 100% Replacement for Fine Aggregate in Concrete," *Materials* 9, no. 6 (June 2016): 440, https://doi.org/10.3390/ma9060440
13. W. H. Langer and B. F. Arbogast, "Environmental Impacts of Mining Natural Aggregate," in *Deposit and Geoenvironmental Models for Resource Exploitation and Environmental Security* (Dordrecht, the Netherlands: Springer, 2002), 151–169, https://doi.org/10.1007/978-94-010-0303-2_8
14. L. H. Anh, F.-C. Mihai, A. Belousova, R. Kucera, K.-D. Oswald, W. Riedel, N. A. Sekar, and P. Schneider, "Life Cycle Assessment of River Sand and Aggregates Alternatives in Concrete," *Materials* 16, no. 5 (March 2023): 2064, https://doi.org/10.3390/ma16052064
15. F. Muleya, B. Mulenga, S. L. Zulu, S. Nwaubani, C. K. Tembo, and H. Mushota, "Investigating the Suitability and Cost-Benefit of Copper Tailings as Partial Replacement of Sand in Concrete in Zambia: An Exploratory Study," *Journal of Engineering, Design and Technology* 19, no. 4 (June 2021): 828–849, https://doi.org/10.1108/JEDT-05-2020-0186
16. A. Bandopadhyay, R. Kumar, and P. Ramachandrarao, eds., *Clean Technologies for Metallurgical Industries (EWM-2002)* (New Delhi, India: Allied Publishers, 2002).
17. S. Zhang, X. Xue, X. Liu, P. Duan, H. Yang, T. Jiang, D. Wang, and R. Liu, "Current Situation and Comprehensive Utilization of Iron Ore Tailing Resources," *Journal of Mining Science* 42, no. 4 (July 2006): 403–408, https://doi.org/10.1007/s10913-006-0069-9
18. A. Umara Shettima, Y. Ahmad, M. Warid Hussin, N. Zakari Muhammad, and O. Eziekel Babatude, "Strength and Microstructure of Concrete with Iron Ore Tailings as Replacement for River Sand," *E3S Web of Conferences* 34 (2018): 1003, https://doi.org/10.1051/e3sconf/20183401003
19. A. Umara Shettima, M. Warid Hussin, Y. Ahmad, and J. Mirza, "Evaluation of Iron Ore Tailings as Replacement for Fine Aggregate in Concrete," *Construction and Building Materials* 120 (September 2016): 72–79, https://doi.org/10.1016/j.conbuildmat.2016.05.095
20. S. Oritola, A. L. Saleh, and A. R. Mohd Sam, "Performance of Iron Ore Tailings as Partial Replacement for Sand in Concrete," *Applied Mechanics and Materials* 735 (2015): 122–127, https://doi.org/10.4028/www.scientific.net/AMM.735.122
21. Z.-X. Tian, Z.-H. Zhao, C.-Q. Dai, and S.-J. Liu, "Experimental Study on the Properties of Concrete Mixed with Iron Ore Tailings," *Advances in Materials Science and Engineering* 2016 (2016): 8606505, https://doi.org/10.1155/2016/8606505
22. Z. Zhang, Z. Zhang, S. Yin, and L. Yu, "Utilization of Iron Tailings Sand as an Environmentally Friendly Alternative to Natural River Sand in High-Strength Concrete: Shrinkage Characterization and Mitigation Strategies," *Materials* 13, no. 24 (December 2020): 5614, https://doi.org/10.3390/ma13245614
23. R. C. Gupta, P. Mehra, and B. S. Thomas, "Utilization of Copper Tailing in Developing Sustainable and Durable Concrete," *Journal of Materials in Civil Engineering* 29, no. 5 (May 2017): 04016274, https://doi.org/10.1061/(ASCE)MT.1943-5533.0001813
24. B. S. Thomas, A. Damare, and R. C. Gupta, "Strength and Durability Characteristics of Copper Tailing Concrete," *Construction and Building Materials* 48 (November 2013): 894–900, https://doi.org/10.1016/j.conbuildmat.2013.07.075

25. A. M. Bhoi, Y. D. Patil, H. S. Patil, and M. P. Kadam, "Feasibility Assessment of Incorporating Copper Slag as a Sand Substitute to Attain Sustainable Production Perspective in Concrete," *Advances in Materials Science and Engineering* 2018 (2018): 6502890, https://doi.org/10.1155/2018/6502890
26. K. S. Al-Jabri, M. Hisada, A. H. Al-Saidy, and S. K. Al-Oraimi, "Performance of High Strength Concrete Made with Copper Slag as a Fine Aggregate," *Construction and Building Materials* 23, no. 6 (June 2009): 2132–2140, https://doi.org/10.1016/j.conbuildmat.2008.12.013
27. *Standard Specification for Portland Cement*, ASTM C150/C150M-22 (West Conshohocken, PA: ASTM International, approved July 1, 2022), https://doi.org/10.1520/C0150_C0150M-22
28. *Drinking Water*, IS 10500 (New Delhi, India: Bureau of Indian Standards, 2012), https://perma.cc/YPE2-Q7ZN
29. *Coarse and Fine Aggregate from Natural Sources for Concrete - Specification (Third Revision)*, IS 383 (New Delhi, India: Bureau of Indian Standards, 2016), https://perma.cc/PTZ5-58DV
30. *Integral Waterproofing Compounds for Cement Mortar and Concrete - Specification*, IS 2645 (New Delhi, India: Bureau of Indian Standards, 2003), https://perma.cc/J8F9-2ZQM
31. *Specification for Concrete Admixtures*, IS 9103 (New Delhi, India: Bureau of Indian Standards, 1999), https://perma.cc/P4YY-U2K9
32. X. Tian, H. Zhang, T. Zhang, and C. A. Fernández, "Alkali-Activated Copper Tailings-Based Pastes: Compressive Strength and Microstructural Characterization," *Journal of Materials Research and Technology* 9, no. 3 (May–June 2020): 6557–6567, https://doi.org/10.1016/j.jmrt.2020.04.043
33. L. Cui, L. Wang, Y. Xu, X. Lou, and H. Wang, "Feasibility Evaluation of Replacing River Sand with Copper Tailings," *Sustainability* 13, no. 14 (July 2021): 7575, https://doi.org/10.3390/su13147575
34. S. Jain, "Green Geopolymers with Copper Tailings for Marine Environments," Azo Materials, 2022, https://perma.cc/UB4K-5E5C
35. *Code of Practice for Preparation and Use of Masonry Mortars (First Revision)*, IS 2250 (New Delhi, India: Bureau of Indian Standards, 1981), https://web.archive.org/web/20231213164338/https://law.resource.org/pub/in/bis/S03/is.2250.1981.pdf
36. *Standard Specification for Mortar for Unit Masonry* (Superseded), ASTM C270-19a (West Conshohocken, PA: ASTM International, approved May 1, 2019), https://doi.org/10.1520/C0270-19A
37. *Methods of Testing Cement-Determination of Strength* (Withdrawn), BS EN 196-1 (London: British Standards Institution, 1995).
38. *Methods of Test for Mortar for Masonry – Determination of Consistence of Fresh Mortar (by Flow Table)*, BS EN 1015-3 (London: British Standards Institution, 1999), https://doi.org/10.3403/01541440
39. *Standard Test Method for Time of Setting of Concrete Mixtures by Penetration Resistance* (Superseded), ASTM C403/C403M-08 (West Conshohocken, PA: ASTM International, approved April 1, 2008), https://doi.org//10.1520/C0403_C0403M-08
40. *Methods of Physical Tests For Hydraulic Cement-Part 6: Determination of Compressive Strength of Hydraulic Cement Other Than Masonry Cement (First Revision)*, IS 4031-6 (New Delhi, India: Bureau of Indian Standards, 1988), https://archive.org/details/gov.in.is.4031.6.1988/page/n5/mode/2up
41. *Methods of Test for Mortar for Masonry – Determination of Dry Bulk Density of Hardened Mortar*, BS EN 1015-10 (London: British Standards Institution, 1999), https://doi.org/10.3403/01905430U
42. M. Safiuddin and N. Hearn, "Comparison of ASTM Saturation Techniques for Measuring the Permeable Porosity of Concrete," *Cement and Concrete Research* 35, no. 5 (May 2005): 1008–1013, https://doi.org/10.1016/j.cemconres.2004.09.017
43. B. B. Das, D. N. Singh, and S. P. Pandey, "A Comparative Study for Determining Pore Volume of Concrete," *The Indian Concrete Journal* 84, no. 12 (December 2010): 7–12, https://web.archive.org/web/20240218160547/https://www.researchgate.net/publication/288071687_A_comparative_study_for_determining_pore_volume_of_concrete
44. *Standard Test Method for Dry and Wet Bulk Density, Water Absorption, and Apparent Porosity of Thin Sections of Glass-Fiber Reinforced Concrete*, ASTM C948-81(2023) (West Conshohocken, PA: ASTM International, approved May 1, 2023), https://doi.org/10.1520/C0948-81R23
45. K. Snehal, B. B. Das, and M. Akanksha, "Early Age, Hydration, Mechanical and Microstructure Properties of Nano-Silica Blended Cementitious Composites," *Construction and Building Materials* 233 (February 2020): 117212, https://doi.org/10.1016/j.conbuildmat.2019.117212
46. J. Zhang and G. W. Scherer, "Comparison of Methods for Arresting Hydration of Cement," *Cement and Concrete Research* 41, no. 10 (October 2011): 1024–1036, https://doi.org/10.1016/j.cemconres.2011.06.003
47. J. W. Bullard, H. M. Jennings, R. A. Livingston, A. Nonat, G. W. Scherer, J. S. Schweitzer, K. L. Scrivener, and J. J. Thomas, "Mechanisms of Cement Hydration," *Cement and Concrete Research* 41, no. 12 (December 2011): 1208–1223, https://doi.org/10.1016/j.cemconres.2010.09.011
48. R. Yu, P. Spiesz, and H. J. H. Brouwers, "Effect of Nano-Silica on the Hydration and Microstructure Development of Ultra-High Performance Concrete (UHPC) with a Low Binder Amount," *Construction and Building Materials* 65 (August 2014): 140–150, https://doi.org/10.1016/j.conbuildmat.2014.04.063
49. L. Soriano, J. Monzó, M. Bonilla, M. M. Tashima, J. Payá, and M. V. Borrachero, "Effect of Pozzolans on the Hydration Process of Portland Cement Cured at Low Temperatures," *Cement and Concrete Composites* 42 (September 2013): 41–48, https://doi.org/10.1016/j.cemconcomp.2013.05.007

50. L. P. Singh, A. Goel, S. K. Bhattacharyya, U. Sharma, and G. Mishra, "Hydration Studies of Cementitious Material Using Silica Nanoparticles," *Journal of Advanced Concrete Technology* 13, no. 7 (2015): 345–354, https://doi.org/10.3151/jact.13.345
51. K. Snehal and B. B. Das, "Acid, Alkali and Chloride Resistance of Binary, Ternary and Quaternary Blended Cementitious Mortar Integrated with Nano-Silica Particles," *Cement and Concrete Composites* 123 (October 2021): 104214, https://doi.org/10.1016/j.cemconcomp.2021.104214
52. K. Snehal and B. B. Das, "Pozzolanic Reactivity and Drying Shrinkage Characteristics of Optimized Blended Cementitious Composites Comprising of Nano-Silica Particles," *Construction and Building Materials* 316 (January 2022): 125796, https://doi.org/10.1016/j.conbuildmat.2021.125796
53. K. Snehal, B. B. Das, and S. Barbhuiya, "Influence of Aggressive Exposure on the Degradation of Nano-Silica Admixed Cementitious Mortar Integrated with Phase Change Materials," *Construction and Building Materials* 335 (June 2022): 127467, https://doi.org/10.1016/j.conbuildmat.2022.127467
54. K. Snehal and B. B. Das, "Effect of Phase-Change Materials on the Hydration and Mineralogy of Cement Mortar," *Proceedings of the Institution of Civil Engineers-Construction Materials* 176, no. 3 (May 2023): 117–127, https://doi.org/10.1680/jcoma.20.00045
55. D. R. Dinger and J. E. Funk, "Particle-Packing Phenomena and Their Application in Materials Processing," *MRS Bulletin* 22, no. 12 (December 1997): 19–23, https://doi.org/10.1557/S0883769400034692
56. Elkem, "Elkem Materials Mixture Analyser (EMMA)," Elkem, https://perma.cc/WZH4-K4QN
57. M. Gou, L. Zhou, and N. W. Y. Then, "Utilization of Tailings in Cement and Concrete: A Review," *Science and Engineering of Composite Materials* 26, no. 1 (2019): 449–464, https://doi.org/10.1515/secm-2019-0029
58. D. Boakye and H. Uzoegbo, "Assessment of Concrete with Pulverized Copper Slag as Partial Replacement of Cement," *Concrete Beton*, no. 139 (November 2014): 14–17.
59. M. Yellishetty, V. Karpe, E. H. Reddy, K. N. Subhash, and P. G. Ranjith, "Reuse of Iron Ore Mineral Wastes in Civil Engineering Constructions: A Case Study," *Resources, Conservation and Recycling* 52, no. 11 (September 2008): 1283–1289, https://doi.org/10.1016/j.resconrec.2008.07.007
60. J. R. Conner, *Chemical Fixation and Solidification of Hazardous Wastes* (New York: Van Nostrand Reinhold, 1990), https://lccn.loc.gov/89016522
61. F. S. Hashem, M. S. Amin, and E. E. Hekal, "Stabilization of Cu (II) Wastes by C_3S Hydrated Matrix," *Construction and Building Materials* 25, no. 8 (August 2011): 3278–3282, https://doi.org/10.1016/j.conbuildmat.2011.03.015
62. M. F. M. Zain, M. N. Islam, S. S. Radin, and S. G. Yap, "Cement-Based Solidification for the Safe Disposal of Blasted Copper Slag," *Cement and Concrete Composites* 26, no. 7 (October 2004): 845–851, https://doi.org/10.1016/j.cemconcomp.2003.08.002
63. H. Zhang, S. Mu, J. Cai, J. Liu, and J. Hong, "The Role of Iron in Cement Hydration Process: From Perspective of Chemical Admixture," *Thermochimica Acta* 722 (April 2023): 179457, https://doi.org/10.1016/j.tca.2023.179457
64. M. A. Largeau, R. Mutuku, and J. Thuo, "Effect of Iron Powder (Fe_2O_3) on Strength, Workability, and Porosity of the Binary Blended Concrete," *Open Journal of Civil Engineering* 8, no. 4 (December 2018): 411–425, https://doi.org/10.4236/ojce.2018.84029
65. Y. Yang, L. Chen, X. Sun, and Y. Mao, "Preparation of Micro-iron Ore Tailings by Wet-Grinding and Its Application in Sulphoaluminate Cement," *Journal of Renewable Materials* 10, no. 4 (2022): 1007–1023, https://doi.org/10.32604/jrm.2022.017372
66. K. Snehal, B. B. Das, and S. Barbhuiya, "Synergistic Effect of Nano Silica on Carbonation Resistance of Multi-blended Cementitious Mortar," *Cement and Concrete Composites* 141 (August 2023): 105125, https://doi.org/10.1016/j.cemconcomp.2023.105125
67. K. Snehal, B. B. Das, and S. Kumar, "Influence of Integration of Phase Change Materials on Hydration and Microstructure Properties of Nanosilica Admixed Cementitious Mortar," *Journal of Materials in Civil Engineering* 32, no. 6 (June 2020): 04020108, https://doi.org/10.1061/(ASCE)MT.1943-5533.0003178
68. D. Zhang, X. Cai, and Y. Shao, "Carbonation Curing of Precast Fly Ash Concrete," *Journal of Materials in Civil Engineering* 28, no. 11 (November 2016): 04016127, https://doi.org/10.1061/(ASCE)MT.1943-5533.0001649
69. V. Corinaldesi, M. Giuggiolini, and G. Moriconi, "Use of Rubble from Building Demolition in Mortars," *Waste Management* 22, no. 8 (December 2002): 893–899, https://doi.org/10.1016/S0956-053X(02)00087-9
70. Z. Zhang, J. Du, and M. Shi, "Quantitative Analysis of the Calcium Hydroxide Content of EVA-Modified Cement Paste Based on TG-DSC in a Dual Atmosphere," *Materials* 15, no. 7 (April 2022): 2660, https://doi.org/10.3390/ma15072660
71. G. Kakali, S. Tsivilis, K. Kolovos, N. Voglis, J. Aivaliotis, T. Perraki, E. Passialakou, and M. Stamatakis, "Use of Secondary Mineralizing Raw Materials in Cement Production. A Case Study of a Wolframite–Stibnite Ore," *Cement and Concrete Composites* 27, no. 2 (February 2005): 155–161, https://doi.org/10.1016/j.cemconcomp.2004.02.037
72. E. Kapeluszna, Ł. Kotwica, and W. Nocuń-Wczelik, "Comparison of the Effect of Ground Waste Expanded Perlite and Silica Fume on the Hydration of Cements with Various Tricalcium Aluminate Content – Comprehensive Analysis," *Construction and Building Materials* 303 (October 2021): 124434, https://doi.org/10.1016/j.conbuildmat.2021.124434
73. M. Hu, X. Zhu, and F. Long, "Alkali-Activated Fly Ash-Based Geopolymers with Zeolite or Bentonite as Additives," *Cement and Concrete Composites* 31, no. 10 (November 2009): 762–768, https://doi.org/10.1016/j.cemconcomp.2009.07.006

74. H. Biricik and N. Sarier, "Comparative Study of the Characteristics of Nano Silica-, Silica Fume-and Fly Ash-Incorporated Cement Mortars," *Materials Research* 17, no. 3 (June 2014): 570–582, https://doi.org/10.1590/S1516-14392014005000054
75. L. Yu, Z. Zhang, X. Huang, B. Jiao, and D. Li, "Enhancement Experiment on Cementitious Activity of Copper-Mine Tailings in a Geopolymer System," *Fibers* 5, no. 4 (December 2017): 47, https://doi.org/10.3390/fib5040047
76. S. Ahmari, K. Parameswaran, and L. Zhang, "Alkali Activation of Copper Mine Tailings and Low-Calcium Flash-Furnace Copper Smelter Slag," *Journal of Materials in Civil Engineering* 27, no. 6 (June 2015): 04014193, https://doi.org/10.1061/(ASCE)MT.1943-5533.0001159
77. I. C. Ferreira, R. Galéry, A. B. Henriques, A. Paula de Carvalho Teixeira, C. D. Prates, A. S. Lima, and I. R. Souza Filho, "Reuse of Iron Ore Tailings for Production of Metakaolin-Based Geopolymers," *Journal of Materials Research and Technology* 18 (May–June 2022): 4194–4200, https://doi.org/10.1016/j.jmrt.2022.03.192
78. A. Jagadisha, K. B. Rao, G. Nayak, and M. Kamath, "Influence of Nano-Silica on the Microstructural and Mechanical Properties of High-Performance Concrete of Containing EAF Aggregate and Processed Quarry Dust," *Construction and Building Materials* 304 (October 2021): 124392, https://doi.org/10.1016/j.conbuildmat.2021.124392
79. A. Y. Patil, N. R. Banapurmath, E. P. Sumukh, M. V. Chitawadagi, T. M. Y. Khan, I. A. Badruddin, and S. Kamangar, "Multi-scale Study on Mechanical Property and Strength of New Green Sand (Poly Lactic Acid) as Replacement of Fine Aggregate in Concrete Mix," *Symmetry* 12, no. 11 (November 2020): 1823, https://doi.org/10.3390/sym12111823
80. P. E. Stutzman, "Scanning Electron Microscopy in Concrete Petrography," in *Materials Science of Concrete, Special Volume: Calcium Hydroxide in Concrete* (Hoboken, NJ: Wiley, 2001), 59–72, https://web.archive.org/web/20231213174249/https://tsapps.nist.gov/publication/get_pdf.cfm?pub_id=860317
81. W. Liu, H. Shi, X. He, S. Pan, Z. Ye, and Y. Wang, "An Application of Optimized Otsu Multi-threshold Segmentation Based on Fireworks Algorithm in Cement SEM Image," *Journal of Algorithms & Computational Technology* 13 (January–December 2019): 1748301818797025, https://doi.org/10.1177/1748301818797025
82. J. Lu, S. Ruan, Y. Liu, T. Wang, Q. Zeng, and D. Yan, "Morphological Characteristics of Calcium Carbonate Crystallization in CO_2 Pre-cured Aerated Concrete," *RSC Advances* 12, no. 23 (2022): 14610–14620, https://doi.org/10.1039/D2RA01901A
83. D. Zhao, J. M. Williams, A.-H. A. Park, and S. Kawashima, "Rheology of Cement Pastes with Calcium Carbonate Polymorphs," *Cement and Concrete Research* 172 (October 2023): 107214, https://doi.org/10.1016/j.cemconres.2023.107214
84. Q. Hu, M. Aboustait, T. Kim, M. T. Ley, J. C. Hanan, J. Bullard, R. Winarski, and V. Rose, "Direct Three-Dimensional Observation of the Microstructure and Chemistry of C_3S Hydration," *Cement and Concrete Research* 88 (October 2016): 157–169, https://doi.org/10.1016/j.cemconres.2016.07.006
85. E. P. Sumukh, S. K. Goudar, and B. B. Das, "Predicting the Service Life of Reinforced Concrete by Incorporating the Experimentally Determined Properties of Steel–Concrete Interface and Corrosion," in *Recent Trends in Civil Engineering* (Singapore: Springer, 2021), 399–417, https://doi.org/10.1007/978-981-15-8293-6_34
86. E. P. Sumukh, S. K. Goudar, and B. B. Das, "A Review on the Properties of Steel-Concrete Interface and Characterization Methods," in *Smart Technologies for Sustainable Development* (Singapore: Springer, 2021), 167–203, https://doi.org/10.1007/978-981-15-5001-0_15
87. S. K. Goudar, E. P. Sumukh, and B. B. Das, "Influence of Marine Environment Exposure on the Engineering Properties of Steel-Concrete Interface," *The Open Civil Engineering Journal* 16 (2022): e187414952210311, https://doi.org/10.2174/18741495-v16-e221026-2022-HT31-3975-5